UNIVERSITY OF PADOVA

DEPARTMENT OF BIOCHEMISTRY

GRADUATE SCHOOL IN BIOCHEMISTRY AND BIOTECHNOLOGIES
SPECIALIZATION AREA IN BIOCHEMISTRY AND BIOPHYSICS
XX CYCLE

ROLE OF MONOAMINE OXIDASE A IN CARDIAC HYPERTROPHY AND TRANSITION TO HEART FAILURE

SCHOOL DIRECTOR: CH.MO PROF. LORENZO A. PINNA

SUPERVISOR: CH.MO PROF. FABIO DI LISA

PhD CANDIDATE: NINA KALUDERCIC

January 31, 2008

INDEX

1 SUMMARY 7

2 INTRODUCTION 15

2.1 Monoamine oxidases 15

2.1.1 Structural features of MAO-A and -B 15

2.1.2 Physiological roles of MAO 16

2.1.3 Tissue distribution of MAO 18

2.1.4 Regulation of MAO gene expression 18

2.1.5 Pathologies related to MAO 19

2.1.6 MAO inhibitors as therapeutic agents 20

2.2 Reactive oxygen species 22

2.2.1 Mechanisms of ROS induced damage 25

2.2.2 Antioxidant defense 26

2.3 Mitochondria: a source and a target of ROS 31

2.3.1 Mitochondria as a source of ROS 31

2.3.2 Mitochondria as ROS targets 33

2.3.3 ROS and mitochondrial permeability transition pore 34

2.4 Mitochondria and cell death 35

2.4.1 Apoptosis 35

2.4.2 Necrosis 36

2.5 Mitochondrial dysfunction in cardiac disease 37

2.6 Hypertrophy and heart failure 39

2.6.1 Major signaling pathways involved in cardiac hypertrophy 41

2.6.2 Role of oxidative stress in cardiac hypertrophy and heart failure. 43

3 AIMS OF THE STUDY 47

4 MATERIALS AND METHODS 49

4.1 Isolation of mitochondria 49

4.2 Determination od protein concentration 49

4.3 Measurement of mitochondrial oxygen consumption 49

4.4 Measurement of hydrogen peroxide formation and MAO activity 50

4.5 Cell cultures 51

4.5.1 HL-1 cardiomyocytes 51

4.5.2 Neonatal rat cardiomyocytes 51
4.6 Fluorescence microscopy 52
4.6.1 Measurement of ROS production in situ 52
4.6.2 Determination of oxidative stress by DHE staining 53
4.6.3 Image analysis 54
4.7 Determination of cell viability 54
4.8 Silencing of MAO-A 55
4.9 Transverse aortic constriction (TAC) 55
4.10 Chronic in vivo treatment with clorgyline 56
4.11 Echocardiography 56
4.12 PCR and real time RT-PCR 57
4.12.1 RNA extraction 57
4.12.2 cDNA synthesis 58
4.12.3 PCR 58
4.12.4 Real time PCR 59
4.13 Protein analysis by gel electrophoresis (Western blot) 61
4.13.1 Samples preparation 61
4.13.2 SDS-polyacrylamide gel electrophoresis (SDS-PAGE) and immunoblot 61
4.13.3 Chemiluminescent detection 63
4.13.4 Densitometry 63
4.14 Statistical analysis 64
5 RESULTS AND DISCUSSION 65
5.1 The role of MAO in the oxidative stress 65
5.1.1 MAO expression at cardiac level 65
5.1.2 Investigation of the effects of MAO inhibitors on mitochondrial function 66
5.1.3 Effect of pharmacological inhibition of MAO on oxidative stress induced by H_2O_2 69
5.1.4 Effect of pharmacological inhibition of MAO on oxidative stress induced by arachidonic acid 72
5.1.5 Effect of genetic inhibition of MAO-A on oxidative stress: siRNA 74
5.2 Involvement of MAO-A in hypertrophy and heart failure 78

5.2.1 Investigation of MAO-A role in *in vitro* hypertrophy 78
5.2.2 Effects of MAO-A inhibition on the development of hypertrophy and congestive heart failure *in vivo* 81
6 CONCLUSIONS 91
7 REFERENCE LIST 93

1 SUMMARY

Oxidative stress has been implicated in numerous pathologies and a number of intracellular sources of ROS have already been identified. Mitochondria and especially mitochondrial respiratory chain, are considered as major intracellular sources of ROS. However, other potential sites responsible for ROS generation are present in the mitochondria and could be equally important, but have not been investigated up to date. In the present thesis, we investigated the role of monoamine oxidases, flavoenzymes located at the level of outer mitochondrial membrane, in the oxidative stress in cardiac myocytes, in relation to cardiac remodeling and transition from hypertrophy to heart failure.

Initially, the expression level of each MAO isoform was determined at the cardiac level. These studies showed that MAO-A is the major isoform present at the cardiac level and that low concentrations of clorgyline (0.05-1 μM) are able to completely prevent H_2O_2 production in the presence of MAO substrates such as tyramine and serotonin. At this concentration clorgyline did not affect mitochondrial function or ROS production by mitochondrial respiratory chain.

To investigate the role of MAO in the oxidative stress, HL-1 cardiomyocytes were treated with H_2O_2 or arachidonic acid to induce an increase in ROS production measured by fluorescent probe Mitotracker Red. Treatment with these agents induced a 1.6- and 1.4-fold increase in oxidative stress, respectively. When cells were pretreated with 1 μM clorgyline, specific inhibitor of MAO-A isoform, this increase in ROS production was reduced or completely prevented. On the contrary, when cells were pretreated with specific MAO-B inhibitor selegiline, no protective effect was observed. This suggests that MAO-A is the major isoform expressed at the cardiomyocyte level and involved in the oxidative stress. To further confirm the specificity of MAO-A inhibition, we genetically silenced the expression of MAO-A by 90% by means of siRNA. Results identical to those obtained using the pharmacological inhibitor clorgyline were observed in siRNA treated cells. These results unequivocally demonstrate that MAO inhibitors are specific and that MAO-A plays an important role in the onset and amplification of oxidative stress.

Given the relevant role of MAO-A in the oxidative stress, we investigated its involvement in hypertrophy and heart failure, a condition strongly favored by increased oxidative burden. *In vitro* studies revealed that MAO-A expression was increased by 2-fold when neonatal rat cardiomyocytes were stimulated with pro-hypertrophic agent norepinephrine (NE) and incubation of the cells with clorgyline reduced the extent of NE-induced hypertrophy. Furthermore, stimulation of MAO-A activity by its substrate tyramine induced the expression of NFAT3 and NFAT4, well known mediators of maladaptive hypertrophy, and this increase was significantly reduced in cells pretreated with clorgyline. These changes were paralleled by an increase in mitochondrial ROS production, which was completely prevented with clorgyline.

To further confirm whether these *in vitro* findings could be of any significance in a more complex, *in vivo* setting, C57Bl6 mice were subjected to transverse aortic constriction (TAC) to induce pressure-overload. This procedure initially results in concentric hypertrophy as a compensatory mechanism for the increase in pressure, leading to eccentric hypertrophy, chamber dilation and heart failure in a long term. MAO-A expression was 3.6-fold higher in mice after 6 weeks of TAC, a time-point associated with chamber dilation and decreased left ventricular (LV) function. Inhibition of MAO-A (CLO) in these mice resulted in reduced hypertrophy and LV dimensions compared to control mice, as calculated LV mass was significantly reduced in CLO group. LV end-diastolic and end-systolic dimensions were 3.5- and 1.3-fold increased in saline treated mice, reflecting chamber remodeling and dilation. This increase in chamber dimensions was absent in CLO group. Cardiac function was also markedly improved in CLO group. Both fractional shortening and ejection fraction were comparable to the values measured in sham operated mice, while they were reduced by 50% in saline treated mice. Differences in morphological and functional data were accompanied also by changes at the molecular level. Fetal gene reprogramming, measured as increase in ANP expression was 4-fold reduced in CLO mice. Reduction in hypertrophy and improvement in cardiac function were also associated with decreased levels of oxidative stress in CLO mice, as determined by DHE staining, and reduced activation of pro-hypertrophic and pro-apoptotic pathways, determined by measuring the levels of activated Akt and cleaved

caspase 3. This suggests that clorgyline exerts its protective effects by reducing the levels of oxidative stress and promoting cell viability.

Taken together, these data demonstrate for the first time that MAO-A plays a major role in the onset and amplification of oxidative stress, contributing to the transition from compensated hypertrophy to dilated cardiomyopathy *in vivo*.

SOMMARIO

Lo stress ossidativo e' stato riconosciuto come uno dei meccanismi alla base di molte patologie e numerosi sono i siti intracellulari di produzione delle ROS. I mitocondri, e la catena respiratoria in particolare, sono considerati una delle principali fonti delle ROS a livello cellulare. Tuttavia, a livello mitocondriale esistono altri potenziali siti di produzione delle ROS.

In questo lavoro di tesi e' stato studiato il ruolo delle monoamino ossidasi (MAO), flavoenzimi localizzati a livello della membrana mitocondriale esterna, nello stress ossidativo a livello dei cardiomiociti ed il loro coinvolgimento nell'ipertrofia del miocardio e nella transizione verso l'insufficienza cardiaca.

Inizialmente e' stato caratterizzato il livello dell'espressione di ciascuna isoforma a livello cardiaco. Questi studi hanno rivelato come la MAO-A sia la prevalente isoforma presente e come la clorgilina, inibitore selettivo della MAO-A, sia in grado di inibire completamente la produzione di H_2O_2 in presenza di substrati delle MAO quali la tiramina e la serotonina, a concentrazioni molto basse (0.05-1 μM). A queste concentrazioni, la clorgilina non influenza ne' la funzionalita' mitocondriale ne' la produzione di H_2O_2 indotta dall'inibizione della catena respiratoria.

Successivamente e' stato determinato il ruolo delle MAO nello stress ossidativo a livello cellulare. La produzione delle ROS, misurata mediante l'utilizzo della sonda Mitotracker Red, e' stata stimolata con H_2O_2 o con acido arachidonico che hanno portato ad un aumento dello stress ossidativo, rispettivamente di 1.6 e 1.4 volte rispetto alle cellule di controllo. Preincubando le cellule con clorgilina 1 μM, tale aumento della produzione delle ROS era ridotto o prevenuto completamente. Al contrario, la preincubazione delle cellule con selegilina, inibitore selettivo della MAO-B, non ha fornito nessuna protezione nei confronti dello stress ossidativo indotto da questi agenti. Inoltre, questi risultati sono stati confermati silenziando l'espressione della MAO-A del 90% mediante siRNA. I risultati ottenuti nelle cellule silenziate per la MAO-A erano identici a quelli ottenuti mediante l'inibizione farmacologica. Percio' si puo' concludere che gli effetti degli inibitori delle MAO sono specifici e che la MAO-A gioca un ruolo determinante nell'instaurarsi dello stress ossidativo.

Successivamente e' stato valutato se le ROS prodotte dalla MAO-A potessero contribuire alla transizione dall'ipertrofia all'insufficienza cardiaca. I dati ottenuti dagli studi *in vitro* hanno dimostrato che il trattamento di miociti neonatali con la norepinefrina portava ad un'aumentata espressione della MAO-A. Inoltre, la preincubazione delle cellule con la clorgilina risultava in una riduzione del grado di ipertrofia indotta dalla norepinefrina. Oltretutto, una persistente attivazione della MAO da parte della tiramina era in grado di indurre l'espressione di NFAT3 e NFAT4, noti mediatori di ipertrofia maladattativa, e la clorgilina era in grado di ridurre significativamente tale aumento. Questo cambiamento era accompagnato da un'aumentata produzione delle ROS a livello mitocondriale, completamente prevenuta dall'incubazione con la clorgilina.

Successivamente e' stato valutato il ruolo della MAO-A nell'ipertrofia *in vivo*. A questo scopo, i topi sono stati sottoposti alla legatura dell'arco aortico per indurre un sovraccarico di pressione. Questo procedimento inizialmente porta ad un'ipertrofia concentrica che poi progressivamente determina ipertrofia eccentrica e cardiomiopatia dilatativa. L'ipertrofia *in vivo* era associata ad un aumento dell'espressione della MAO-A di 3.6 volte rispetto ai topi di controllo dopo 6 settimane dalla legatura. Il trattamento di questi topi con la clorgilina e' risultato in una riduzione del grado di ipertrofia: la massa del ventricolo sinistro era significativamente ridotta nel gruppo trattato con la clorgilina. Le dimensioni del ventricolo sinistro in sistole e diastole erano aumentate di 3.5 e 1.3 volte rispettivamente nei topi trattati con il veicolo, indicando la progressione verso la cardiomiopatia dilatativa. Questo aumento era assente nel gruppo trattato con la clorgilina, i cui valori sono rimasti paragonabili a quelli del gruppo di controllo. Anche la funzione ventricolare era migliorata nel gruppo trattato con la clorgilina: l'accorciamento frazionale e la frazione di eiezione erano paragonabili ai valori osservati nel gruppo di controllo, mentre nel gruppo trattato con il veicolo erano ridotti del 50%. I dati morfologici e funzionali erano accompagnati da differenze anche dal punto di vista molecolare. L'espressione di ANF, indice della riprogrammazione genica, era ridotta di 4 volte nel gruppo trattato con la clorgilina rispetto ai topi trattati con la soluzione fisiologica. La riduzione dell'ipertrofia ed il miglioramento della funzione ventricolare erano accompagnati da una diminuzione dello stress ossidativo, misurato mediante l'utilizzo della sonda fluorescente DHE. Infine, la clorgilina ha determinato una ridotta

attivazione delle cascate di segnale pro-ipertrofiche e pro-apoptotiche, definite mediante la misurazione dei livelli di Akt attivata e della caspasi 3. Questo suggerisce che la prevenzione della disfunzione ventricolare e l'inibizione della dilatazione del ventricolo sono probabilmente dovute alla riduzione del grado di morte cellulare.

L'insieme di questi dati dimostra per la prima volta che la MAO-A, rivestendo un ruolo centrale nello stress ossidativo, determina la transizione dall'ipertrofia alla cardiomiopatia dilatativa.

2 INTRODUCTION

2.1 Monoamine oxidases

2.1.1 Structural features of MAO-A and -B

Monoamine oxidases are flavoenzymes located within the outer mitochondrial membrane, responsible for the oxidative deamination of neurotransmitters and dietary amines. They exist in two isoforms, MAO-A and B, distinguished by different substrate specificity and inhibitor sensitivity. MAO-A and MAO-B genes are both located closely on the X chromosome and present identical intron-exon organization. Exon 12 codes for the covalent FAD binding site and is the most conserved exon, showing 94% amino acid identity between MAO-A and B[1, 2]. These two enzymes present 70% homology in their primary sequence[3, 4] and both contain the pentapeptide Ser-Gly-Gly-Cys-Tyr, where the obligatory cofactor FAD is covalently bound through a thioether linkage to the cysteine residue[3, 5], namely Cys406 in MAO-A and Cys397 in MAO-B[6, 7]. This flavin moiety is the only redox factor necessary for the explication of their activity. MAO-A and B are integrated proteins of the outer membrane of mitochondria, anchored through a C-terminal α-helix segment that protrudes from the basal face of the structure and is highly hydrophobic, therefore facilitating the insertion into the membrane. For that reason, their crystallization has been difficult and human enzymes have been crystallized only recently[8, 9] (Fig.1). MAO-B crystallizes as a dimer, with each monomer presenting a C-terminal membrane bound domain, FAD binding domain and a substrate binding domain[8, 10]. For a substrate molecule to reach the flavin center, it must first negotiate a protein loop at the entrance to one of the two cavities before reaching the flavin coenzyme. The first cavity is very hydrophobic in nature and has been named the "entrance cavity". Separating the "entrance cavity" from a similarly hydrophobic "substrate cavity" is an Ile199 side chain which serves as a gate between the two cavities. At the end of the "substrate cavity" is the FAD coenzyme[11]. In contrast to human MAO-B, human MAO-A crystallizes as a monomer[9]. It has only single substrate binding cavities with protein loops at the entrances of either cavity. The

single cavity in MAO-A displays a rounder shape and is larger in volume than the substrate cavity in MAO-B. Analysis of residue side chains in either active site shows the substrate to have less freedom for rotation in the MAO-B site than in MAO-A. The structural basis for this difference can be partially attributed to the conformational differences of the 200-215 residue segment that constitutes the "cavity shaping loop" in both isoforms. This loop is in a more extended conformation in MAO-A and in a more compact conformation in MAO-B.

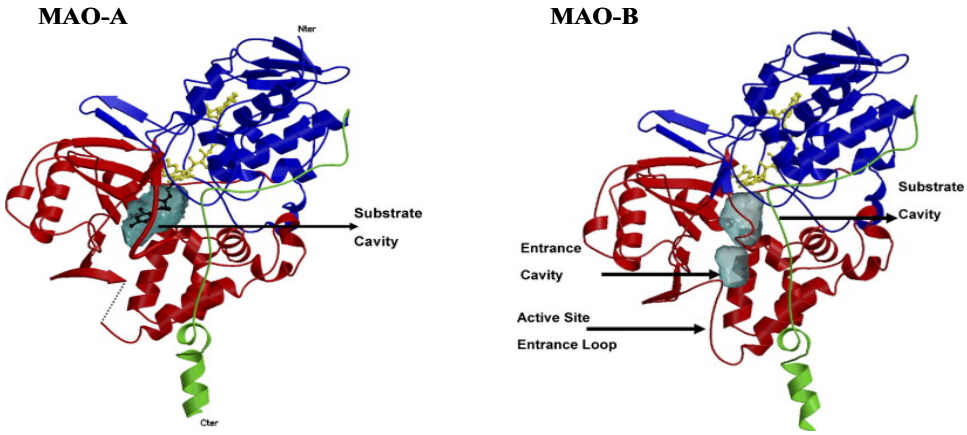

Figure 1. Ribbon diagram of human MAO-A and –B structures. The covalent flavin moiety is shown in a ball and stick model in yellow. The flavin binding domain is in blue, the substrate domain in red and the membrane binding domain in green. *From Edmondson et al, 2007.*

2.1.2 Physiological roles of MAO

In peripheral tissues, MAO are involoved in the oxidative catabolism of amines from the blood and in preventing the entry of dietary amines into the circulation. In the central and peripheral nervous system, intraneuronal MAO-A and –B protect neurons from exogenous amines, terminate the actions of amine neurotransmitters and regulate the contents of intracellular amine stores. MAO-A catalyses preferentially the oxidative deamination of norepinephrine (NE) and serotonin (5-HT) and is inhibited by low concentrations of clorgyline. In contrast, MAO-B has major affinity for phenylethylamine and benzylamine, and is inhibited by selegiline[12]. Both isoforms catalyze the deamination of dopamine, tyramine, octopamine and tryptamine and are inhibited by pargyline.

MAO catalyze the following reaction:

$$RCH_2NR'R'' + O_2 + H_2O \rightarrow RCHO + NR'R'' + H_2O_2$$

Kinetic studies have shown that the binding of the amine group to the enzyme precedes the binding of oxygen[13]. In a first moment, the reduction of the cofactor FAD yields an aldehyde intermediate and ammonia, while in a second moment the oxidized form of the prosthetic group is restored with the concomitant production of hydrogen peroxide.

$$RCH_2NH_2 + MAO \rightarrow RCHO + NH_3 + MAO\text{- reduced}$$

$$MAO\text{- reduced} + O_2 \rightarrow MAO + H_2O_2$$

The aldehyde intermediate is rapidly metabolized to corresponding acid by the action of aldehyde dehydrogenase.

The main physiological role of MAO is the degradation of endogenous monoamine neurotransmitters and dietary amines, such as tyramine, that, if not properly catabolized, may cause hypertensive crises[12]. Similarly, MAO-B in the microvessels and blood-brain barrier has a protective function acting as a metabolic barrier, preventing the entrance of false and potentially toxic neurotransmitters.

Deletion of MAO-A and MAO-B genes has proven their important roles in neurotransmitter metabolism and behavior. MAO-A knockout mice have elevated brain levels of 5-HT, NA and, to a lesser extent, dopamine[14], whereas only 2-phenylethylamine is increased in MAO-B knockout mice[12]. Both MAO-A and –B knockout mice show increased reactivity to stress, similar to that observed after administration of non-selective MAO inhibitors. However, these studies, and the deletion of both MAO-A and MAO-B in a rare form of human Norrie disease, indicate that MAO is not essential for survival[15]. Gene deletion has shown that MAO-A activity is important during development. A compulsive-aggressive behavior results from lack of MAO-A function in humans[16] and mice[17]. This effect, which might reflect the importance of serotonin during development, can be mimicked by the administration of MAO-A inhibitor clorgyline during the early postnatal period. Studies of MAO-A knockout mice have also shown the

maintenance of serotonin levels to be important for the normal development of thalamocortical axons and the aggregation of neurons to form barrels[18].

2.1.3 Tissue distribution of MAO

The distribution of MAO in various tissues of different species has been investigated by use of specific inhibitors, immunohystochemistry, enzyme autoradiography and *in situ* hybridization[19-21]. Their distribution has been particularly studied in the brain, where MAO-A has been prevalently found in noradrenergic neurons whereas MAO-B has been detected in serotoninergic and histaminergic neurons and in glial cells[22-25]. In peripheral tissues, MAO-A has been found in placenta, liver, intestine and thyroid gland, while platelets, liver and kidney contain mainly MAO-B. Human cardiomyocytes contain both enzymes, although MAO-A is the predominant isoform[26-28].

2.1.4 Regulation of MAO gene expression

Differential expression of MAO-A and B genes might be due to differences in their core promoter regions. MAO-B, but not MAO-A, expression is regulated by mitogen-activated protein kinase (MAPK) pathway that includes protein kinase C, the small G protein Ras, ERK, MEK3, MEK7, ERK2, JNK1 and p38[29]. Progesterone, testosterone, corticosterone and glucocorticoids increase the levels of MAO-A, but have little or no effect on MAO-B[30, 31]. Likewise, MAO-A is elevated in the endometrium, reproductive tissue and the brain where levels of progesterone are high during the oestrous cycle. Castration leads to a threefold increase in MAO-A activity and this increase can be prevented the administration of oestradiol or testosterone.

Both MAO-A and B promoters are GC-rich and are regulated by Sp1 family of transcription factors[29]. However, they have distinctly different features. MAO-B gene, but not MAO-A gene, has TATA box and MAO-B promoter contains two clusters of overlapping Sp1 sites, the CACCC repressor element (Fig. 2). Another interesting feature of human MAO-A and MAO-B promoters is the fact that they appear to have the cAMP responsive element, which suggests

that their expression might be regulated by the activation of receptors coupled to adenylate cyclase[32, 33].

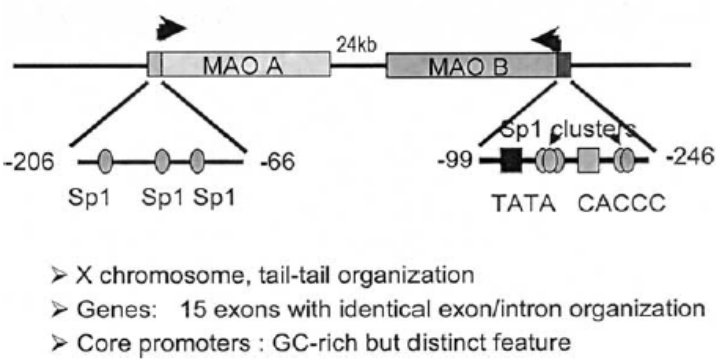

Figure 2. Schematic representation of MAO-A and –B genes and their core promoters. *From Shih et al, 2004.*

2.1.5 Pathologies related to MAO

The roles of MAO in terminating the actions of neurotransmitters/dietary amines in central and peripheral nervous system and in the extraneuronal tissue have been extensively studied. In contrast, less attention has been given to the products of their activity. The monoamine catabolism byproducts are aldehydes, ammonia and H_2O_2, a reactive oxygen species that could be toxic *per* se at high concentrations[34, 35] or it could generate hydroxyl radical when in the presence of Fe^{2+}. MAO are involved in numerous pathologies, in particular in neuronal and psychiatric disorders. MAO-B appears to be involved in the loss of dopaminergic neurons that occurs in Parkinson's disease, most likely due to the increased dopamine catabolism, resulting in elevated production of reactive oxygen species responsible for the oxidative damage at the level of nigrostriatal neurons. Indeed, MAO-B inhibition has been proven to afford neuroprotection[36]. An increase in MAO-B activity in brain is also associated with diseases such as Alzheimer's or Huntington's disease. Depression, panic attacks and personality disorders are also associated with changes in dopaminergic, noradrenergic and serotoninergic neurotransmission, which are regulated by both isoforms of MAO.

Besides their implication in neurodegenerative diseases, MAO role has been recently described in post-I/R cardiac damage[37]. MAO-A has been demonstrated to be an important source of ROS in receptor-independent apoptotic effects of serotonin in isolated cardiomyocytes and post ischemic myocardial injury. Also, MAO-A can promote cell apoptosis through ROS-dependent sphingosine kinase inhibition with accumulation of ceramide[38]. MAO-dependent ROS increase is also relevant *in vitro* for serotonin-induced myocyte hypertrophy[39]. MAO-A mediated ROS production can also induce mitogenic signaling in smooth muscle cells. The latter may involve metalloproteinase MMP-2 activation[40], likely contributing to vascular wall remodeling. Interestingly, MAO-A ability to produce ROS appears to increase with ageing, a process often accompanied by congestive heart failure[41].

2.1.6 MAO inhibitors as therapeutic agents

The therapeutic potential of MAO inhibitors has been discovered in the early '50s, when antituberculosis treatment with iproniazid was shown to improve the mood and inhibit MAO activity[42]. A wide range of MAO inhibitors is available today and these are proving to have a therapeutic value in several diverse conditions, including affective disorders, neurodegenerative diseases, stroke and ageing. MAO inhibitors are distinguished by their specificity for each isoform and by the nature of their binding to the enzyme[3, 43]. They can be classified in three groups:

- Irreversible and non selective inhibitors, such as phenelzine and tranylcypromine;
- Irreversible and selective inhibitors, such as selegiline for MAO-B and clorgyline for MAO-A;
- Reversible and selective MAO-A inhibitors, such as moclobemide.

MAO inhibitors have been used for decades for the treatment of depression[44, 45]. The antidepressant properties result from selective MAO-A inhibition in the CNS, which leads to increased brain levels of dopamine, noradrenalin and serotonin. Some of the non selective irreversible inhibitors, such as phenelzine and tranylcypromine, are still in clinical use along with the

reversible MAO inhibitors moclobemide, befloxatone and toloxatone. As levels of MAO-B are increased in patients with Parkinson's disease, MAO-B inhibitor selegiline has been used as a dopamine sparing agent or as adjunct to L-DOPA and has been shown to be effective both as an adjuvant to L-DOPA and as monotherapy[46]. Combination of MAO-B inhibitor with cholinesterase inhibitor is beneficial for the treatment of Alzheimer's disease[47]. Selegiline has also been shown to reduce the peripheral tissue damage that results from cardiac failure[48], and that arising in the brain from cerebral ischemia[49] in animal models. This protective effect has been attributed to a decrease in hydrogen peroxide production generated by MAO during ischemia/reperfusion. Selegiline has also been shown to increase Bcl2 to Bax ratio and activate the translocation of anti-apoptotic protein kinases, PKCα and PKCε[50, 51], although the mechanisms leading to these effects are not completely elucidated yet. However, protective outcome following selegiline treatment hasve also been observed at concentrations lower then those required for MAO-B inhibition, suggesting that they may be independent of MAO-B inhibition.

The following are irreversible MAO inhibitors used in this study:

- Pargyline (N-methyl-propargylbenzylamine): non selective inhibitor, able to inhibit both, MAO-A and B;

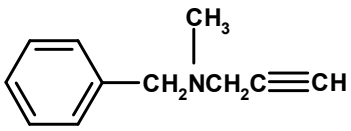

- Clorgyline (N-methyl-N-propargyl-3-(2,4-dichlorphenoxy)propylamine): selective inhibitor of MAO-A;

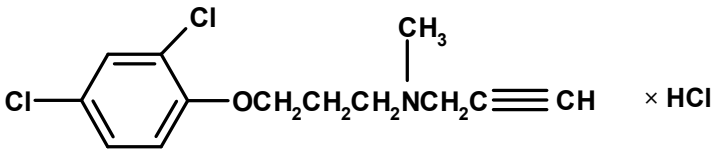

- Selegiline (N-α-Dimethyl-N-2propyonil-benzene-ethanolamine): selective inhibitor of MAO B.

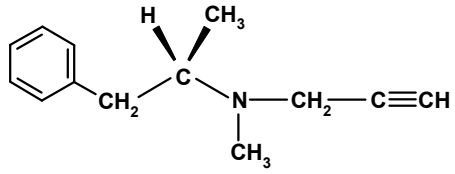

Considering the important role of MAO as a source of H_2O_2 that has been described both in the brain as well as in the heart following post-I/R cardiac injury, development of MAO inhibitors may represent an important tool for the treatment of various diseases.

2.2 Reactive oxygen species

Oxygen is an indispensable molecule for the aerobic organisms; however it can become toxic when it is partially reduced. In that case, unstable and reactive intermediates are formed and it has been demonstrated that these are involved in numerous pathophysiological conditions, such as ageing, cancer, myocardial infarction, neurodegenerative diseases and many others[52].

ROS can be formed by a variety of mechanisms, including generation during oxidative phosphorylation in the mitochondria as a byproduct of normal cellular aerobic metabolism[53, 54]. Atoms or molecules with unpaired electrons are designated as free radicals and are highly reactive entities that can readily participate in a variety of chemical and biochemical reactions. In the aerobic environment, cells generate energy at mitochondrial level, reducing molecular oxygen to water during the electron transport in the mitochondrial respiratory chain. Molecular oxygen is found in nature as a diatomic molecule, presenting two unpaired electrons with parallel spin in its outermost shell (triplet oxygen) and this configuration makes it non reactive and weak oxidant. The complete reduction of one molecule of oxygen to 2 molecules of water, requires the transfer of 4 electrons. However, partial reduction of oxygen during this process can generate reactive intermediates, known as reactive oxygen species[55, 56]. The products of partial oxygen reduction are following:

- Singlet oxygen ($^1O_2$): it is the molecular oxygen in its first excited singlet state, presenting both electrons in the same molecular orbitale with paired spins. It is generated by the transfer of energy to the triplet molecular oxygen and it has been postulated to be an important intermediate in a range of biological systems. Most commonly, singlet oxygen is formed following exposure to UV or visible light in the presence of chromophores that can act as sensitising agents, such as tryptophan, tyrosine or cystine. However, it can also be formed by a range of peroxidase enzymes or during the reaction of H_2O_2 with peroxynitrite. $^1O_2$ interacts with a wide range of biological targets, including DNA, RNA, proteins, lipids and sterols. In proteins, it has been demonstrated to interact with tryptophan, tyrosine, histidine, methionine and cyteine side chains[57].
- Superoxide anion ($O_2^{\bullet-}$): it is formed following a single electron donation to molecular oxygen

$$O_2 + e^- \rightarrow O_2^{\bullet-}$$

The biological toxicity of superoxide is due to its capacity to inactivate iron-sulfur cluster containing enzymes, critical in a wide variety of metabolic pathways, thereby liberating free iron in the cell, which can undergo Fenton chemistry and generate the highly reactive hydroxyl radical. In its HO_2 form (hydroperoxyl radical), superoxide can also initiate lipid peroxidation of polyunsaturated fatty acids. It also reacts with carbonyl compounds and halogenated carbons to create toxic peroxy radicals. Superoxide can also react with nitric oxide (NO) to form $ONOO^-$. As such, superoxide is one of the main causes of oxidative stress. Superoxide can also produce hydrogen peroxide through a dismutation reaction catalyzed by superoxide dismutase. However, this may be followed by hydroxyl radical formation through the Haber-Weiss reaction[58].

$$2O_2^{\bullet-} + H^+ \rightarrow O_2 + H_2O_2$$
$$O_2^{\bullet-} + H_2O_2 \rightarrow OH^{\bullet-} + OH^- + O_2$$

- Hydrogen peroxide (H_2O_2): it is formed when two electrons are donated to molecular oxygen according to the reaction:

$$O_2 + 2e^- + 2H^+ \rightarrow H_2O_2$$

Otherwise, it is formed by superoxide anion dismutation. It is lipid soluble and thus able to diffuse across membranes.

Depending on concentrations, H_2O_2 can act as a signaling molecule. However, it can be a dangerous species for the biological systems, as in the presence of ions such as Fe^{2+} e Cu^+, it can generate highly reactive hydroxyl radical according to the Fenton reaction[59]:

$$H_2O_2 + Fe^{2+} \rightarrow OH^{\bullet -} + OH^- + Fe^{3+}$$

- Hydroxyl radical ($OH^{\bullet -}$): it is the most dangerous reactive oxygen specie for the biological sytems, as it can not be neutralized by enzymatic antioxidant systems. It is formed following the reaction of H_2O_2 with ferrous ions during the Fenton reaction, as a product of a reaction between superoxide and H_2O_2 (Haber-Weiss reaction) or during water radiolysis induced by electromagnetic irradiation. The hydroxyl radical cannot be eliminated by an enzymatic reaction, as this would require its diffusion to the enzyme's active site. As diffusion is slower than the half-life of the molecule, it will react with any oxidizable compound in its vicinity. It can damage virtually all types of macromolecules: carbohydrates, nucleic acids (mutations), lipids (lipid peroxidation) and amino acids (e.g. conversion of Phe to m-Tyrosine and o-Tyrosine). The only means to protect important cellular structures is the use of effective repair systems and antioxidants.

2.2.1 Mechanisms of ROS induced damage

ROS can be dangerous for biological systems for their capacity to interact with numerous macromolecules, such as proteins, lipids and DNA. Three types of reaction can occur: extraction of a $H^{\bullet}$ from an organic molecule; addition of $OH^{\bullet}$; and electron transfer. The common feature of these reactions is that the initial reaction is always amplified due to the formation of another radical, resulting in a chain reaction. Therefore, these molecules are dangerous not only because of their reactivity, but also because of their capacity to trigger chain reactions, resulting in formation of secondary radicals that can diffuse and lead to the propagation of the damage. These reactions can terminate only when free radicals are in the presence of a similar molecule, able to neutralize them (i.e. scavenger), or an enzymatic system, able to metabolize them.

Following are some examples of ROS induced damage:

- Oxidative damage of DNA: ROS have been shown to be mutagenic[60], an effect that should be derived from chemical modification of DNA. A number of alterations (e.g., cleavage of DNA, DNA-protein cross links, oxidation of purines, etc.) are due to reactions with ROS, especially hydroxyl radical. If the DNA-repair systems are not able to immediately regenerate intact DNA, a mutation will result from erroneous base pairing during replication. This mechanism may partly explain the high prevalence of cancer in individuals exposed to oxidative stress. Of the oxidative lesions, the most dangerous are double-strand breaks, as these are difficult to repair and can produce point mutations, insertions and deletions from the DNA sequence, as well as chromosomal translocations[61].

- Oxidative damage to proteins: once they are oxidized, proteins cannot be repaired. Extensive studies have revealed that oxidized proteins are recognized by proteases and completely degraded (to amino acids), and entirely new replacement protein molecules are then synthesized de novo[62]. It seems that oxidized amino acids within oxidatively modified proteins are eliminated or used as carbon sources for

intermediate metabolism and consequent energy synthesis. Because an oxidatively modified protein may contain only two or three oxidized amino acids, it seems probable that most of the amino acids from an oxidized and degraded protein are re-utilized for protein synthesis. Thus, during oxidative stress many proteins that are synthesized are likely to contain a high percentage of recycled amino acids. During periods of particularly high oxidative stress the proteolytic capacity of cells may not be sufficient to cope with the number of oxidized protein molecules being generated. A similar problem may occur in ageing, or with certain disease states, when proteolytic capacity may decline below a critical threshold of activity required to cope with normal oxidative stress levels[63]. Under such circumstances oxidized proteins may accumulate and cross-link with one another or form extensive hydrophobic bonds. Such aggregates of damaged proteins are detrimental and may lead to cell dysfunction[64].

- Oxidative damage of lipids: membrane lipids are rich in polyunsaturated fatty acids that can easily be oxidized by ROS, because of their multiple double bonds. Such oxidation is also involved in the generation of atherosclerotic plaques[65]. Their oxidation results in excess formation of carbonyl compounds, such as prostanoid and aldehydes that are toxic metabolites that can impinge on numerous pathologies.

2.2.2 Antioxidant defense

ROS are constantly formed, even under physiological conditions. However, their production is counterbalanced by several cellular mechanisms, including enzymatic and non enzymatic pathways[61]. Among the best characterized enzymatic systems are:

1. Superoxide dismutase (SOD): in eukaryotic cells, $O_2^{\bullet -}$ can be metabolized to hydrogen peroxide by two metal-containing SOD isoenzymes, an 80-kDa tetrameric Mn-SOD present in mitochondria[66], and the cytosolic 32-

kDa dimeric Cu/Zn-SOD[67]. In the reaction catalyzed by SOD, two molecules of superoxide form hydrogen peroxide and molecular oxygen and are thereby a source of cellular hydrogen peroxide. The reaction catalyzed by SOD is extremely efficient, limited in essence only by diffusion.

$$O_2^{\bullet-} + O_2^{\bullet-} + 2H^+ \xrightarrow{SOD} H_2O_2 + O_2$$

2. Catalase (CAT): catalases of many organisms are mainly heme-containing enzymes. This enzyme is predominantly localized in mitochondria and peroxisomes, where it catalyzes the dismutation of hydrogen peroxide to water and molecular oxygen:

$$2H_2O_2 \xrightarrow{CAT} 2H_2O + O_2$$

Catalase is also involved in detoxifying different substrates, e.g., phenols and alcohols, via coupled reduction of hydrogen peroxide:

$$H_2O_2 + RH_2 \xrightarrow{CAT} 2H_2O + R$$

One antioxidative role of catalase is to lower the risk of hydroxyl radical formation from H_2O_2 via the Fenton-reaction catalyzed by Cu^+ or Fe^{2+} ions. Catalase binds NADPH, which protects the enzyme from inactivation and increases its efficiency.

3. Glutathione peroxidase (GPx) and glutathione reductase (GR): There are at least four different GPx in mammals (GPx1–4), all of them containing selenocysteine[68]. GPx1 and GPx4 (or phospholipid hydroperoxide GPx) are both cytosolic enzymes abundant in most tissues. GPx is also localized at the mitochondrial level where it catalyzes the reduction of H_2O_2 produced by Mn-SOD, using glutathione as substrate. This system affords protection against low levels of oxidative stress, while catalase is more efficient when oxidative burden is increased[69]. They can also reduce other peroxides (e.g., lipid peroxides in cell membranes) to alcohols. In physiological conditions, reduced glutathione (GSH) is used for the

reduction of H_2O_2 and is transformed into oxidized glutathione (GSSH). GR is the flavoenzyme that restores GSH.

4. Thioredoxin system: is constituted from thioredoxin (Trx), thioredoxin reductase (TrxR) and NAPDH and operates as a powerful protein disulfide oxidoreductase system. Trx is a 12 kDa protein containing a dithiol-disulfide active site. It acts as antioxidant by facilitating the reduction of other proteins by cysteine thiol-disulfide exchange. The oxidized Trx is reduced and regenerated by the flavoenzyme TrxR, in a NADPH-dependent reaction. Thioredoxins act as electron donors to peroxidases and can catalyze the regeneration of many antioxidant molecules, including ubiquinone, lipoic acid and ascorbic acid (Fig. 3).

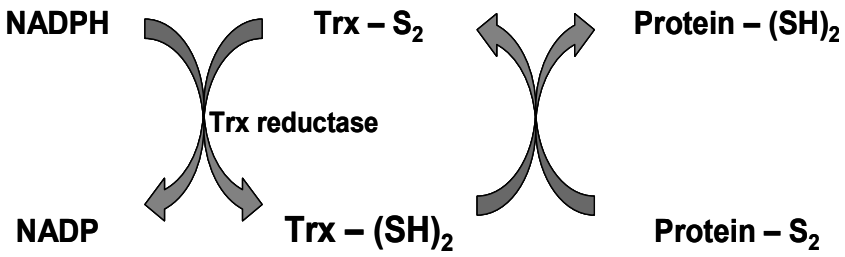

Figure 3. The thioredoxin system. Thioredoxin reduces disulfides and methionine sulfoxides in oxidizied proteins with a concomitant oxidation of cysteine moieties. The corresponding disulfide is, in turn, reduced by thioredoxin reductase.

Besides the enzymatic systems, there is a number of intracellular antioxidants that act as scavengers:

1. Vitamin E (α-tocopherol): it is the most studied of the fat-soluble antioxidant vitamins as it has the highest bioavailability, with the body preferentially absorbing and metabolizing this form. It has been suggested that the α-tocopherol form is the most important lipid-soluble antioxidant, and that it protects membranes from oxidation by reacting with lipid radicals produced in the lipid peroxidation chain reaction[70].

$$\text{VitE-OH} + \text{LOO}^{\bullet} \rightarrow \text{VitE-O}^{\bullet} + \text{LOOH}$$

This removes the free radical intermediates and prevents the propagation reaction from continuing. The tocopheril radical that is formed is fairly stable, not reactive and does not contribute to the formation of other radicals. The oxidized α-tocopheroxyl radicals produced in this process may be recycled back to the active reduced form through reduction by ascorbate, retinol or ubiquinol. The functions of the other forms of vitamin E are less well-studied, although γ-tocopherol is a nucleophile that may react with electrophilic mutagens, and tocotrienols may have a specialized role in neuroprotection.

2. Vitamin C (ascorbic acid): it is a water soluble antioxidant found in both animals and plants. In cells, it is maintained in its reduced form by reaction with glutathione, which can be catalyzed by protein disulfide isomerase and glutaredoxins[71]. Ascorbic acid is a reducing agent and can easily donate a hydrogen atom form the hydroxil group bound to carbon 2 and thereby neutralize reactive oxygen species such as hydrogen peroxide.

3. Glutathione (GSH): is a cysteine containing peptide (Glu-Cys-Gly). Glutathione has antioxidant properties since the thiol group in its cysteine moiety is a reducing agent and can be reversibly oxidized and reduced. In cells, glutathione is maintained in the reduced form by the enzyme glutathione reductase and in turn reduces other metabolites and enzyme systems as well as reacting directly with oxidants (Fig. 4). Due to its high concentration and its central role in maintaining the cell's redox state, glutathione is one of the most important cellular antioxidants.

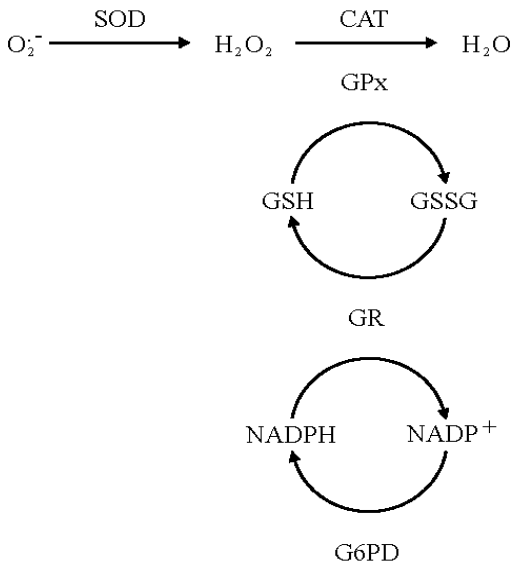

Figure 4. Glutathione redox cycle. Hydrogen peroxide is reduced to water with the concomittant oxidation of glutathione (GSH) to glutathione disulfide (GSSG). Considering that intracellular amounts of GSH are limited, the reduced form is restored by the action of the enzyme glutathione

4. Bilirubin: is the end product of heme catabolism in mammals that can efficiently scavenge peroxyl radical[72]. Heme oxygenase is a stress-inducible enzyme that catalyzes the degradation of heme to liberate, among other products, biliverdin IX, a hydrophilic compound that is reduced by biliverdin reductase to bilirubin. There is evidence that bilirubin can protect cells and LDL against lipid peroxidation and contribute to the antioxidant capacity of jaundiced newborn infants. The antioxidant mechanism by which bilirubin deactivates peroxyl radicals, the main chain-carrying radicals in lipid peroxidation, is still not completely clear. However, the proposed mechanisms include hydrogen atom transfer from the methylene at position C-10 to peroxyl radicals, peroxyl radical addition to the pyrroles, and single electron transfer.

5. Uric acid: derives from purine metabolism and it is the most abundant aqueous antioxidant in humans. Local concentrations of uric acid have been shown to increase during acute oxidative stress and ischemia, likely reflecting a compensatory mechanism that confers protection against increased free radical activity[73]. Uric acid is particularly effective in

quenching hydroxyl, superoxide and peroxynitrite radicals, and may serve a protective physiological role by preventing lipid peroxidation.

2.3 Mitochondria: a source and a target of ROS

2.3.1 Mitochondria as a source of ROS

The majority of intracellular ROS production is derived from mitochondria. Although the mitochondrial electron transport chain is a very efficient system for the production of ATP, the very nature of the alternating one-electron oxidation-reduction reactions it catalyzes, predisposes each electron carrier to side reactions with molecular oxygen. The superoxide anion radical ($O_2^{\bullet -}$) and hydrogen peroxide (H_2O_2), the products of the univalent and bivalent reduction of oxygen (O_2) respectively, are produced during normal aerobic metabolism and constitute physiological intracellular metabolites. The physiological rate of the mitochondrial production of $O_2^{\bullet -}$ and H_2O_2 associated with the electron transfer chain is dependent on the mitochondrial metabolic state: the resting mitochondrial state 4 is characterized by a relatively slow rate of respiration and no availability of ADP and is associated with a relatively high rate of $O_2^{\bullet -}$ and H_2O_2 production, probably as a consequence of the high reduction state of the components of the respiratory chain[62]. Conversely, the active mitochondrial respiratory state 3, with a high rate of oxygen uptake and ample availability of ADP, shows a relatively slow rate of $O_2^{\bullet -}$ and H_2O_2 production due to the highly oxidized state of the components of the respiratory chain.

Evidence indicates that, *in vitro*, mitochondria convert 1–2% of the oxygen molecules consumed into superoxide anions. Given that these initial estimates were made on isolated mitochondria in the presence of high, non-physiological concentrations of oxygen, the *in vivo* rate of mitochondrial superoxide production is undoubtedly considerably less. The production of mitochondrial superoxide radicals occurs primarily at two discrete points in the electron transport chain, namely at complex I (NADH dehydrogenase) and at complex III (ubiquinone–cytochrome *c* reductase)[74, 75] (Fig. 5). However, given the potentially harmful effects of ROS, mitochondria possess efficient systems for

their neutralization. Superoxide produced at the level of Complex I and III is rapidly transformed into H_2O_2 by Mn-SOD present in the mitochondrial matrix.

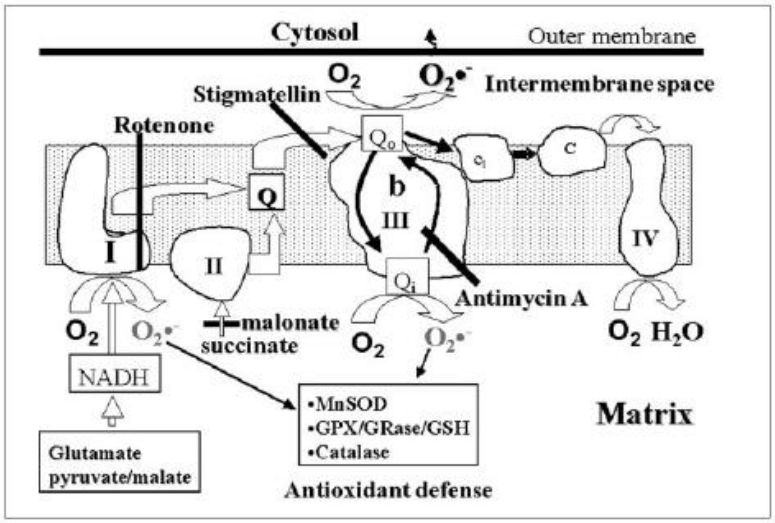

Figure 5. Schematic representation of mitochondrial respiratory chain. The major sources of ROS are Complex I and III. Mitochondrial antioxidant systems are localized in the matrix.

ROS production in mitochondria is however increased in various pathological conditions such as hypoxia, ischemia and reperfusion, ageing and following the inhibition of the mitochondrial respiratory chain.

An additional source of ROS, not linked to respiration, is provided by p66Shc. This protein, which localizes in part within mitochondria, catalyzes the electron transfer from cytochrome c to oxygen. The consequent ROS formation has been linked to PTP opening and apoptosis[76]. Interestingly, the ablation of its gene results in lifespan prolongation along with increased resistance to oxidative stress. Indeed, fibroblasts lacking p66Shc displayed reduced formation of ROS in response to oxidative stress inducing agents. Conversely, p66Shc overexpression resulted in enhanced stress induced apoptosis[76-78]. Further studies have shown that p66Shc$^{-/-}$ mice display a decreased susceptibility to hindlimb ischemia, as well as a reduction in high-fat induced atherosclerosis[79].

Another example of mitochondrial ROS generation at sites other than the respiratory chain is MAO, as described previously in the Introduction. It is noteworthy that the brain intramitochondrial H_2O_2 generation obtained during the monoamine oxidase-catalyzed oxidative deamination of tyramine is 48-fold

higher than that originating during the oxidation of substrates *via* complex II of the electron transfer chain in the presence of antimycin A[62].

2.3.2 Mitochondria as ROS targets

Besides being a major site for ROS production, mitochondria are compromised by severe and/or prolonged oxidative stress. Proteins, lipids and nucleic acids can be altered by ROS resulting in covalent changes that profoundly affect their structure and function. Although repair processes efficiently preserve mitochondrial structure and function, this line of defense is evaded by ROS attack occurring under conditions of severe or prolonged oxidative stress, such as post-ischemic reperfusion or aging, so that damage of mitochondrial components becomes detectable.

Results from different experimental models indicate that complex I is highly susceptible to ROS attack. Its activity is decreased by oxidative stress in a process that is prevented *in vitro* by thiol antioxidants. This type of protein oxidation involving cysteinyl residues is, at least theoretically, reversible. Triptophan residues represent another "hot spot" for oxidation potentially resulting in complex I dysfunction[80]. Complex I activity has also been shown to be inhibited by nitrosylation of tyrosine residues induced by peroxynitrite[81]. These forms of protein oxidation result in irreversible covalent modifications of the affected proteins. In these cases the modified proteins have to be removed by proteolysis and replaced by de novo synthesis. As discussed in the previous sections, errors in these repair processes result in the accumulation of oxidized products.

Since complex I is also considered to be the major site for ROS production within the respiratory chain[82, 83], a vicious cycle is likely set up, eventually resulting in cell death. Interestingly, irreversible damage appears to correlate more with ROS formation than with respiratory chain dysfunction[84].

Functional and structural alterations are also a likely result of lipoperoxidation. A highly susceptible target is cardiolipin[85]. This phospholipid, which is especially abundant in the inner mitochondrial membrane, binds to cytochrome *c* and has been suggested to modulate the activity of crucial proteins,

such as cytochrome oxidase and adenine nucleotide translocase. Cardiolipin oxidation has been proposed to contribute to complex I impairment and cytochrome *c* release. The mitochondrial impairment that is acutely induced by oxidative derangements of lipids and proteins can be transformed into a long-term dysfunction by ROS-induced alterations of mitochondrial DNA[86].

2.3.3 ROS and mitochondrial permeability transition pore

Sustained oxidative stress can cause the opening of PTP resulting in uncoupling of the oxidative phosphorylation. The PTP is a Ca^{2+} and voltage-dependent high-conductance channel located in the inner mitochondrial membrane[87]. At physiological values of membrane potential it is present in a closed conformation. Following changes in membrane potential, PTP can open, allowing passive diffusion of solutes with molecular masses up to about 1.5 kDa. The main regulatory site for the PTP opening appears to be a voltage sensor present at the membrane level that can be affected by effectors such as Ca^{2+}, shifting the membrane potential over the threshold value and thereby promoting the opening of the pore, or Mg^{2+} and ADP, which favors the closed conformation[88].

The most important physiological effectors are:

1. Divalent cations: The permeability transition is greatly favored by accumulation of Ca^{2+} ions in the matrix, while it is counteracted by Me^{2+} ions like Mg^{2+}, Sr^{2+} and Mn^{2+}[89]
2. $\Delta\psi_m$: At physiological membrane potentials the pore favors the closed state, while it can be opened by membrane depolarization[90], although this is not invariably the case. Many effectors are able to modify the threshold voltage. Thus, PTP opening can be obtained by either depolarization, or by changing the threshold potential. On the other hand, mitochondrial depolarization might prevent PTP opening by reducing Ca^{2+} uptake. This concept might hold valid for ischemic tissues.
3. Inorganic phosphate favors PTP opening.

4. Protons: The probability of PTP opening is sharply increased below and above pH 7.4. The inhibitory effect of H^+ is exerted from the matrix side of the inner membrane[89], and is linked to reversible protonation of histidyl residues.
5. Adenine nucleotides: The probability of pore opening is decreased by adenine nucleotides, ADP being more potent than ATP[91].
6. redox state: the redox state of pyridin nucleotides and mitochondrial pool of glutathione can affect P and S sites of the PTP[92]. Indeed, their oxidation can influence the threshold potential facilitating the opening of the pore.

Oxidative stress has long been known to increase the probability of pore opening[86, 93]. This occurs because of the collapse of the electrochemical gradient present at the level of inner mitochondrial membrane and uncoupling between the electron transport and ATP synthesis. Recent findings indicate that PTP can be targeted by p66Shc-produced peroxides resulting in apoptosis. Interestingly, in isolated cardiomyocytes ROS-induced PTP opening was followed by a burst of mitochondrial ROS formation[94]. This event is known as ROS induced ROS release and may result in release of cytochorme c in the cytoplasm. Indeed, the opening of PTP leads to the release of mitochondrial proteins such as cytochrome c, SMAC and APAF-1 that activate the caspases leading to apoptosis.

2.4 Mitochondria and cell death

Mitochondria and ROS play an important role in the processes of cell death that may occur through phenomena of apoptosis and necrosis.

2.4.1 Apoptosis

Apoptosis is a physiological process that normally occurs in multicellular organisms, also known as programmed cell death. It plays a major role in the maintenance of tissue homeostasis, organogenesis and tissue remodeling during the embryogenesis in the vertebrates[95]. This process is also important for the elimination of potentially dangerous cells like autoreactive lymphocytes T, virus infected or cancer cells. Indeed, the purpose of this form of cell death is to

eliminate unnecessary cells from the organism, through a series of coordinated and programmed events[96].

Apoptosis contributes to homeostasis which is achieved when the rate of cell proliferation in the tissue is balanced by cell death. However, disturbance of this equilibrium contributes to the development of numerous pathologies. Some diseases, such as cancer, are associated with apoptosis inhibition and survival of abnormal cells[97]. Others instead, are associated with higher rates of apoptosis and excessive cell death. For example, increase in apoptosis contributes to loss of cardiomyocytes following ischemic injury during myocardial infarction[98] or limphocyte depletion, as in AIDS[99]. Therefore, the organism must orchestrate a complex series of controls to keep homeostasis tightly controlled, a process that is ongoing for the life of the organism and involves many different types of cell signaling pathways.

Apoptosis involves a series of biochemical events that lead to a variety of morphological changes, including blebbing, changes to the cell membrane such as loss of membrane asymmetry and attachment, cell shrinkage, nuclear fragmentation, chromatin condensation, and chromosomal DNA fragmentation (1-4).

Mitochondria play an important role in apoptosis through a release of proteins that initiate the pro-apoptotic cascade. These involve SMACs (second mitochondria-derived activator of caspases), which are released into the cytosol following an increase in permeability and bind to *inhibitor of apoptosis proteins* (IAPs) deactivating them and preventing them from arresting the apoptotic process. Cytochrome c is also released from mitochondria following PTP[100]. Once it is released it binds with APAF-1 and ATP, which then bind to *pro-caspase-9* to create a protein complex known as apoptosome. The apoptosome cleaves the pro-caspase to its active form of caspase-9, which in turn activates the effector *caspase-3*.

2.4.2 Necrosis

Necrosis is accidental form of cell death usually induced by exogenous insults that induce irreversible injury. There are many causes of necrosis including prolonged exposure to injury, infection, cancer, infarction, poisons and

inflammation. Exogenous agents that may induce necrosis include physical, chemical and biological factors. Finally, genetic mutations or damage to cell genome can also result in necrosis.

This form of cell death begins with cell swelling, chromatin digestion, and disruption of the plasma and organelle and membranes. Late necrosis is characterized by extensive DNA hydrolysis, vacuolization of the endoplasmic reticulum, organelle breakdown, and cell lysis. The release of intracellular content after plasma membrane rupture is the cause of inflammation in necrosis. The main difference between necrosis and apoptosis is that necrosis is a gene- and ATP-independent process, i.e. it does not require ATP, mRNA or protein synthesis. Recent studies have demonstrated that variations in ATP content can determine which form of cells death is going to occur[101]. Therefore, mitochondria appear to play an important role in these processes, considering that maintenance of the electrochemical gradient across the membrane necessary for the ATP synthesis is essential for cell survival. Indeed, reduced ATP synthesis appears to be one of the factors responsible for the occurrence of necrosis in syndromes like ischemia/reperfusion, oxidative stress or calcium ionophors induced toxicity[102]. A crucial role in the evolution of cell injury is also to be attributed to the direction of operation of the F_1F_0 ATPase, which may turn mitochondria into the major consumers of cellular ATP in the futile attempt to restore the proton electrochemical gradient[93].

2.5 Mitochondrial dysfunction in cardiac disease

For its function, the heart is highly dependent on oxidative energy generated in mitochondria, primarily by fatty acid β-oxidation, electron transport chain and oxidative phosphorylation. Mitochondria are abundant in energy demanding cardiac tissue, where they constitute over one third of the cardiomyocyte cellular volume. Energy production in mitochondria depends on genetic factors that modulate normal mitochondrial function including enzyme activity and cofactor availability and on environmental factors, such as the availability of fuels (i.e. sugars, fats and proteins) and oxygen. In the postnatal and adult heart, fatty acids are the primary energy substrate for heart muscle ATP generation by oxidative

phosphorylation and the mitochondrial respiratory chain, the most important source of cardiac energy. The primary ATP-utilizing reactions in the myocyte involve actomyosin ATPase in the myofibril, the Ca^{2+}-ATPase in the sarcoplasmic reticulum (SERCA), and the Na^{+},K^{+}-ATPase in the sarcolemma. Over 75% of ATP produced by mitochondrial oxidative phosphorylation is used preferentially to support myocyte contractile activity. Indeed, mitochondria appear to be clustered at sites of high ATP demand and are organized into highly ordered elongated bundles, regularly spaced between rows of myofilaments and in contact with the sarcoplasmic reticulum (SR). Moreover, structural contacts between the SR and mitochondria, revealed by electron microscopy, appear to support the coordination between these organelles at the level of Ca^{2+} homeostasis and regulation of ATP production.

Considering its dependence on mitochondrial bioenergetics and metabolism, the heart is especially vulnerable to mitochondrial derangements[91, 103]. Insufficient cellular oxygenation leads to the inhibition of electron flow through the respiratory chain and impairment of energy conservation and oxidative metabolism. Inhibition of respiratory chain prevents ADP phosphorylation into ATP at the level of F_1F_0ATP synthase for the loss in protonmotive force composed of membrane potential and proton gradient. Indeed, if the proton gradient is not generated, F_1F_0ATP synthase couples ATP hydrolysis with proton pumping to maintain the mitochondrial membrane potential. The net result is that mitochondria cease to represent the main source of intracellular ATP and become the powerful system for hydrolyzing glycolytically produced ATP[104]. Moreover, mitochondrial Ca^{2+} homeostasis is also altered following, for example, ischemia/reperfusion injury. Upon reperfusion, active accumulation of Ca^{2+} within the mitochondrial matrix due to the rise in cytosolic Ca^{2+}, can cause an overload resulting in PTP opening, mitochondrial depolarization and cell death[105, 106]. As described in the previous sections, these changes are also accompanied by increased ROS formation due to the inhibition of the respiratory chain.

Besides ischemia/reperfusion injury, mitochondrial dysfunction contributes also to the development of heart failure. In this chronic syndrome, cardiac mitochondria present structural abnormalities and are increased in number[107]. The activity of respiratory chain complexes and ATP synthase are reduced[108-110], the regulation of oxidative phosphorylation by the phosphate acceptors AMP, ADP

and creatine is impaired[111], and the levels of uncoupling proteins, which cause mitochondria to produce heat rather then ATP, is increased[112]. In particular, myocardial tissue from paced dogs that develop congestive heart failure similar to that observed in human dilated cardiomyopathy, displayed markedly reduced activities of respiratory complex III and ATP synthase[113]. Furthermore, the reduction in the ATP synthase activity was identified as both, an early and a persistent event in the development of heart failure. These data are of crucial importance considering that reduced activity levels of mitochondrial bioenergetic enzymes including selected respiratory enzymes and mitochondrial creatine kinase was found also in patients with heart failure[114]. Moreover, the failing human heart has a 25–30% decline in ATP levels as determined in human biopsy specimens[115].

Genetic approach has also provided many insights into the involvement of mitochondria in heart failure. Gene ablation in mice targeting a wide spectrum of genes encoding specific mitochondrial proteins results in severe cardiomyopathy. Adenine nucleotide translocator knockout mice and mice lacking cytochrome c oxidase subunit VIa-H both display dilated cardiomyopathy and severe cardiac ATP deficiency[116, 117], which is thought to underlie the resulting cardiac phenotype. In addition, cardiac specific overexpression of genes that mediate the expression and control of cardiac energy metabolism, i.e. PGC1-α and PPAR-α, has been shown to lead to severe cardiac dysfunction and marked changes in mitochondrial structure and function[118, 119].

The finding that Mn-SOD deficient mice develop ROS toxicity and dilated cardiomyopathy[120], underlines the importance of ROS in this pathology and mitochondria as their source and target. Identification of sources of ROS that contribute to mitochondrial dysfunction may represent a new therapeutical tool for the treatment of cardiac disease.

2.6 Hypertrophy and heart failure

The adjustment of cardiac mass to hemodynamic load is a fundamental characteristic of the heart. Any sustained increase in hemodynamic function caused by either physiologic activity or pathologic alterations in the cardiovascular system eventually leads to changes in cardiomyocyte size.

Physiologic hypertrophy occurs in response to adaptive changes, such as vigorous exercise, and its mechanism is primarily filling and emptying the heart to provide beat-to-beat adjustment that enables the heart to meet short-term changes in hemodynamics and to equalize the output of the two ventricles. Cardiomyocyte hypertrophy develops also as a response to an increase in biomechanical stress that can be extrinsic, such as in arterial hypertension or valvular heart disease, or intrinsic, as in familial hypertrophic cardiomyopathy. Although this may provide initial salutary compensation to the stress, sustained hypertrophic stimulation can become maladaptive, resulting in a significant increase in the risk for sudden death or progression to heart failure (Fig 6).

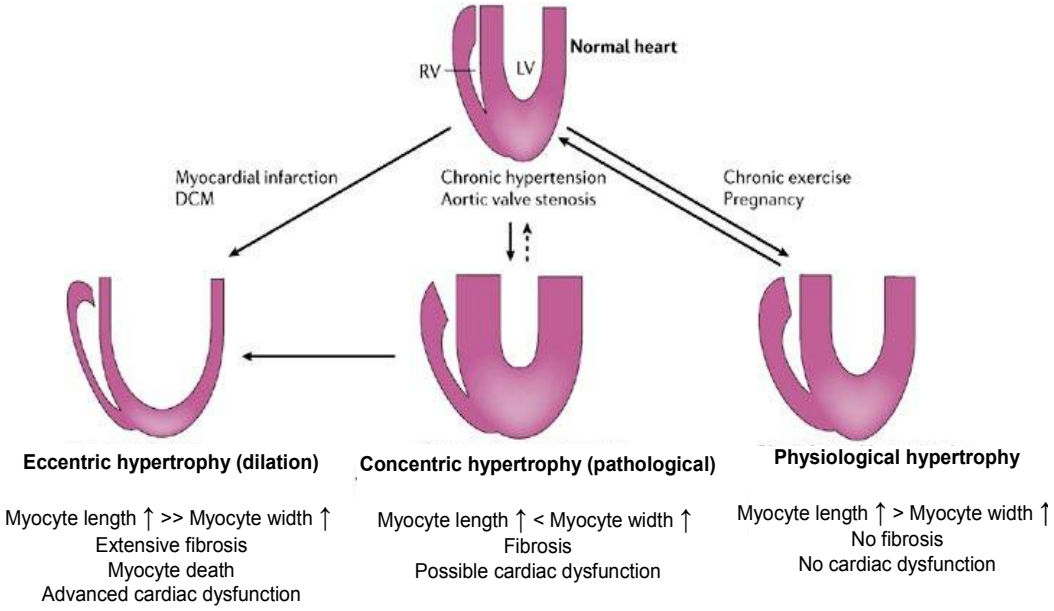

Figure 6. Types of cardiac hypertrophy. Chronically elevated blood pressure causes compensatory concentric hypertrophy, thereby lessening the effect of increased afterload on wall tension. Eccentric hypertrophy is another form of pathological hypertrophy, characterized by increased chamber dimension and thinning of the wall. *Modified from Heineke et al, 2006.*

The defining features of hypertrophy are an increase in cardiomyocyte size, enhanced protein synthesis and a higher organization of the sarcomere. These changes in cellular phenotype are preceded and accompanied by the re-induction of the so called fetal gene program[121]. Indeed, an increased and sustained hemodynamic load is translated into a series of cell signals that cause the nucleus to initiate the formation of new proteins and cause subtle but important

ultrastructural changes. These changes include, for example, isoform shift in the myosin heavy chains, from high ATPase α isoform to the slower β isoform, isoform shifts in the myosin light chains and replacement of cardiac α-actin with skeletal α-actin.

Pathological hypertrophy is associated with progressive ventricular remodeling through alterations in the extracellular matrix that eventually impact cardiac function and energy use and cause increased rates of myocyte cell death by apoptotic and necrotic mechanisms[122]. Pathological hypertrophy initially produces concentric hypertrophy in which the ventricular wall and septum thicken with a net decrease in ventricular chamber dimensions. This remodeling is associated with a greater increase in myocyte width than length. However, chronic maladaptive changes lead to eccentric hypertorphy or dilatation and include progressive dilatation, myocyte death and fibrosis. Eccentric and concentric hypertrophy and impaired contractility and relaxation are the most important causes of abnormal cardiac performance in patients with chronic heart failure.

2.6.1 Major signaling pathways involved in cardiac hypertrophy

A number of signaling pathways that mediate the hypertrophic response is activated following increase in load (Fig. 7), as a result increased release in endocrine and paracrine factors that mediate their effects through tyrosine kinase or G protein coupled receptors[121]. The stimulation of the latter results in increase in intracelluar calcium and activation of calcineurin, a protein phosphatase that dephosphorylates and activates nuclear factor of activated T cell (NFAT), which in turn activates the transcription factors MEF2C and GATA4 to induce protein synthesis. Constitutive activation of calcineurin in transgenic mouse hearts is sufficient to induce massive cardiac enlargement and eventually heart failure[123]. Similar results were obtained by overexpression of NFAT3, whereas mice lacking the NFAT4 gene showed reduced myocardial growth in response to the activated calcinuerin transgene, aortic banding and angiotensin II infusion[124]. The calcineurin pathway is integrated with other pathological signaling systems including those controlled by stress responsive MAPK and calcium-dependent kinases, such as PKC or CaMK[125-127]. Interestingly, PKC inhibition by gene

targeting has shown that they are not involved in regulation of cardiac hypertrophy. However, its overexpression can reduce cardiac hypertrophy in transgenic mice, indicating that these proteins are not the primary regulators of this process[128].

PI3Ks are enzymes associated with cell growth, proliferation and survival[129]. Activation of the α isoform is associated with physiological hypertrophy with preserved ventricular function[130]. However, PI3Kγ has been shown to to contribute to the generation of pathological hypertrophy and cardiac dysfunction following pressure overload[131]. One of the principal targets of PI3K is Akt. Although Akt signaling is important for the physiological growth of the heart, sustained overexpression of activated Akt leads to pathological cardiac hypertrophy with dilation[132]. Whether these different outcomes may be due to differential activation/inhibition of the effectors downstream of Akt, is not clear. The mediators of PI3K/Akt induced hypertrophy are regulator of protein synthesis called mammalian target of rapamycin (mTOR) and GSK-3β. The latter is inhibted by Akt, whereas its activation is able to antagonize pathological hypertrophy[133].

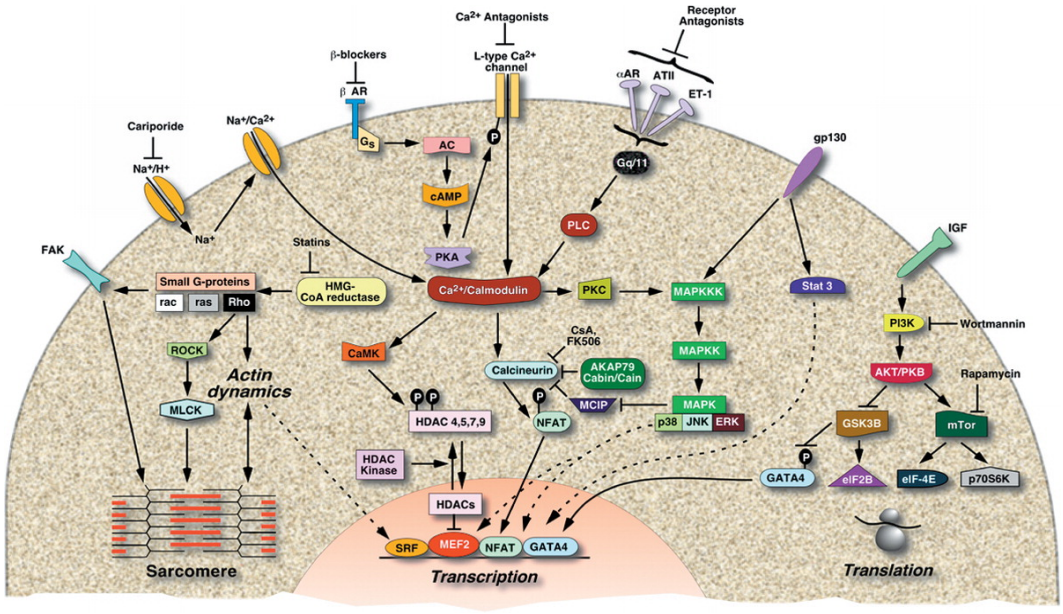

Figure 7. Signaling pathways involved in cardiac hypertrophy. *From Frey et al, 2003.*

Pathological hypertrophy stimulated by peptide growth factors is mediated by RAS, a monomeric G protein, which stimulates MAPK pathways. MAPK signaling consists of a sequence of successfully functioning kinases that ultimately result in phosphorylation and activation of p38, c-Jun N-terminal kinases (JNK) and ERK. Mice with cardiac specific activation of ERK1/2 develop stable concentric hypertrophy[134], suggesting that ERK-dependent signaling may constitute a pathway for physiological hypertrophy. However, it has also been shown that this pathway can enhance the transcriptional activity of NFAT[135], indicating the existance of a crosstalk with the calcineurin/NFAT circuit. Different responses are mediated by p38. Specific activation of p38 does not result in cardiac hypertrophy, but rather in rapid development of heart failure characterized by reduced functional performance, fibrosis and thinning of ventricular wall[136]. Similar phenotype was observed also following JNK activation[137]. These kinases are also known as stress-activated protein kinases, therefore it is likely that their activation alters the hypertrophic response as a consequence of their capability to induce myocyte apoptosis and necrosis. Most of these pathways participate in both adaptive and maladaptive growth responses, but some pathways appear to favor physiological hypertrophy, while others mediate pathological concentric hypertrophy and progressive dilation. However, because of extensive cross-talk between proliferative signaling pathways, it is difficult to assign a specific function to one or another signaling mechanism.

2.6.2 Role of oxidative stress in cardiac hypertrophy and heart failure

A growing body of evidence suggests that ROS and oxidative stress may contribute to the pathogenesis of myocardial remodeling and failure[138-140]. A number of signaling pathways that mediate hypertrophic response, matrix remodeling and cellular dysfunction can be modulated by ROS, which have been demonstrated to activate a broad variety of hypertrophy signaling kinases and transcription factors.

Recent studies suggest that hypertrophic effects of angiotensin are mediated through ROS generation. Nakamura et al reported that AT II induced ROS generation in neonatal rat myocytes and that pretreatment with antioxidants could

abolish AT II-mediated hypertrophy[141]. It was also demonstrated that this mechanism involves H_2O_2 dependent activation of Ras/Raf/ERK MAP kinase pathway and activation of the transcription factor NFκB. Norepinephrine (NE) interacts with α- and β-adrenergic receptors and both receptor subtypes have been implicated in NE-induced ROS generation and hypertrophy[142]. In neonatal rat myocytes, NE increased the level of intracellular ROS and this effect was inhibited by α-adrenergic receptor blockade and antioxidants. Incubation with catalase, was able to prevent NE-induced increase in ROS and RNA and protein content.

In cardiomyocytes, relatively low levels of H_2O_2 have been demonstrated to activate ERK1/2 MAPK and the stimulation of protein synthesis. Although the mechanism is still unclear, this process also seems to involve PKC activation, another kinase involved in prohypertrophic signaling. However, high levels of H_2O_2 stimulate JNK, p-38 and Akt to induce apoptosis[143], and could contribute to ventricular remodeling through this mechanism. Another MAPK family member linking ROS and hypertrophy is ASK-1, a redox-sensitive kinase upstream of JNK and p-38. ASK-1 overexpression activates NFkB to stimulate hypertrophy, whereas its genetic silencing inhibits hypertrophy induced by AT II, NE and endothelin-1[144]. Moreover, overexpression of ASK-1 induces apoptosis in cardiomyocytes and ASK-1 knockout mice demonstrated attenuated ventricular remodeling in response to pressure overload, a finding attributed in part to a reduction in apoptosis[145].

ROS have also potent effects on extracellular matrix, stimulating cardiac fibroblast proliferation and activating MMPs[146], effects central to fibrosis and cardiac remodeling. MMPs are generally secreted in an inactive form and are activated post-translationally by ROS from targeted interactions with critical cysteins in the propeptide autoinhibitory domain[147]. ROS are also able to influence contractile function by modifying proteins central to excitation-contraction coupling[148]. This includes modification of critical thiol groups on the ryanodine receptor to enhance its open probability, suppression of L-type calcium channel current and oxidative interaction with the sarcoplasmatic reticular Ca^{2+} ATPase to inhibit Ca^{2+} uptake (ref).

A number of intracellular sources have already been identified up to date. These include NADPH oxidase, xantine oxidase, mitochondrial respiratory chain and NOS that, when uncoupled, can become a powerful ROS generator. Despite the fact that experimental studies strongly support a key role of oxidative stress in the pathophysiology of cardiac hypertrophic remodeling and dysfunction, clinical data testing these findings remain scarce. More specific targeting of the source of oxidative stress may ultimately provide more effective approaches to reversing cardiac remodeling.

3 AIMS OF THE STUDY

The aim of this study was to investigate the role of monoamine oxidase A and B in the oxidative stress in the cardiomyocytes and to determine whether these enzymes are involved in *in vivo* hypertrophy and transition to heart failure.

One of the major hypotheses was that MAO are involved in the oxidative stress, and more specifically, that the isoform A of the enzyme plays a major role. This was assessed by two approaches: a classical pharmacological approach, using selective inhibitors for each isoform, and by genetic approach, silencing the protein expression of MAO-A, the main cardiac isoform. The efficacy and specificity of MAO inhibitors were also determined in isolated mitochondria, assessing whether they can affect mitochondrial function.

Given the encouraging results demonstrating the involvement of MAO-A in the oxidative stress, we hypothesized that MAO A-derived ROS might be involved in cardiac hypertrophy and likely contribute to the transition toward heart failure. To this aim, we assessed whether direct stimulation of MAO-A activity was able to trigger pro-hypertrophic stimuli *in vitro*. Furthermore, we investigated the effects of pharmacological MAO-A inhibition on cardiac structure and function in an *in vivo* model of hypertrophy and congestive heart failure induced by pressure overload.

4 MATERIALS AND METHODS

4.1 Isolation of mitochondria

Mitochondria were isolated from mice hearts. Hearts were rapidly excised and immediately placed in ice cold isolation buffer containing 225mM mannitol, 75mM sucrose, 1mM EGTA, 20mM Hepes, pH 7.4, rapidly minced and homogenized using Polytron homogenizer at low speed. The homogenate was centrifuged at 500 g for 10 minutes at 4°C (Sorvall, SS34), the supernatant is filtered through a 150 μm mesh and centrifuged again at 10 800 x g for 10 minutes at 4°C. The pellet was resuspended in isolation buffer without BSA, centrifuged at 8 000 g for 10 min and the final pellet was resuspended in a small volume of isolation buffer and stored on ice until the analysis.

4.2 Determination od protein concentration

Protein concentration was determined by biuret reaction. 20 μl of mitochondrial suspension were added to a mixture containing 1 ml of H_2O_2, 1.5 ml of biuret reactive and 0.5 ml of 1% sodium deoxycholate. To accelerate the reaction, tubes were immersed in boiling water for 1 minute and then cooled. The absorbance was then measured at 540 nm and the background determined measuring the absorbance in the absence of mitochondria was subtracted. Protein concentration was calculated from a standard curve determined using bovine serum albumin as a standard.

4.3 Measurement of mitochondrial oxygen consumption

Standard medium was used for the experiments containing 250 mM sucrose, 1 mM KH_2PO_4, 20 μM EGTA, 10 mM MOPS, pH 7.4, and 5/2.5 mM glutamate/malate as substrates or 5 mM succinate in the presence of 2 μM rotenone. Oxygen consumption was determined polarographically using Clark

electrode. The electrode is constituted from a negatively charged platinum cathode and a positively charged silver anode immersed in a saturated KCl solution divided by a membrane selectively permeable to oxygen. Initially the medium was added to the chamber maintained at 37°C and continuously stirred. After the equilibration of the medium, 0.5 mg/ml mitochondria were added and oxygen consumption was followed for 2 minutes. Test compounds at different concentrations were added and after 3 minutes FCCP was added to induce maximal respiration and oxygen consumption monitored for another 3 minutes.

4.4 Measurement of hydrogen peroxide formation and MAO activity

Hydrogen peroxide formation was determined using Amplex Red. The assay is based on the detection of hydrogen peroxide generated during substrate catabolism in a horseradish peroxidase (HRP) coupled reaction using 10-acetyl-3,7-dihyrdoxyphenoxazine (Amplex Red reagent, Molecular Probes) (Fig. 8).

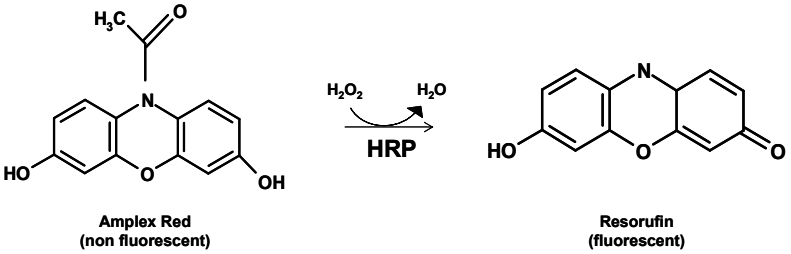

Figure 8. The mechanism of Amplex Red oxidation.

For the measurements of hydrogen peroxide production from the respiratory chain, mitochondria were incubated in a standard medium in the presence of 10 μM Amplex Red reagent and 15 μg HRP. The reaction was started by the addition of 5 mM succinate or 1 μM Antimycin A and monitored for 10 minutes at 37°C using a Perkin Elmer LS-50B fluorimeter at the 544/590 nm excitation/emission wavelengths. The velocity of H_2O_2 production was calculated from a calibration curve obtained adding known amounts of H_2O_2.

MAO activity was measured in the mitochondrial fraction following the same protocol. To discriminate between MAO A and B activity specific substrates and inhibitors for each isoform were used. Mitochondrial proteins were incubated

in 100 mM phosphate buffer with Amplex Red and HRP. The reaction is started adding 10, 50 or 100 μM tyramine or serotonin and fluorescence intensity was recorded for 10 minutes. Parallel samples were run in the absence of substrate determine an eventual increase in fluorescence not due to MAO A activity.

4.5 Cell cultures

4.5.1 HL-1 cardiomyocytes

HL-1 cardiomyocytes, a stabilized cell line of cardiac myocytes deriving form murine tumor atrial cells, were used for the measurement of oxidative stress in situ. Cells were cultured in the Claycomb medium (JRH Biosciences) added with 4 mM L-Glutamine (Invitrogen), 100 U/ml penicillin and streptomycin (Invitrogen), 50 μM norepinephrine (Sigma) and 10% inactivated fetal calf serum (FCS, Invitrogen) to maintain the differentiated phenotype of the cells. Cells were grown at a density of 0.64-1.24 x 10^5 cells/cm^2 in flasks coated with 1 μg/ml fibronectin and 0,02% gelatin to permit the adhesion of cells to the flask and maintained in the incubator at 37°C and 5% CO_2. For the experiments, cells were treated with 0.05% p/v trypsin-EDTA to detach them form the flasks, centrifuged at 180 x g for 5 minutes and counted. 5 x 10^5 cells/well were plated in 6 well plates, in which a sterile 24 mm diameter glass cover slide was introduced, previously treated with fibronectin and gelatin as described above. Cells were kept in the incubator for 24 hours prior to the experiments.

4.5.2 Neonatal rat cardiomyocytes

Ventricular myocytes were isolated from 1 – 3 days old Wistar rats. Hearts were excised from rats anaesthetized with isofluorane, transferred to an ice cold, sterile solution (solution A) containing 140 mM NaCl, 4.8 mM KCl, 1.2 mM $MgSO_4$, 4 mM $NaHCO_3$, 1.2 mM NaH_2PO_4, 12.5 mM D-glucose, 10 mM HEPES, pH 7.4, and washed twice. Hearts were then cut into small fragments. Tissue fragments were further dissociated by incubating them with an enzyme solution containing 285 μg collagenase type II (Worthington, USA) and trypsin

(Invitrogen) per milliliter solution A at 37°C for 15 min for 5 times, under continuous stirring. Pooled cell suspensions were pelleted by centrifugation (15 min, 300 x *g*). To purify them, cells were resuspended in growth medium consisting of DMEM (Invitrogen) supplemented with 10% fetal bovine serum (Sigma) and antibiotics (100 U/ml penicillin and 100 µg/ml streptomycin), and pre-plated for 90 minutes. After this incubation, only fibroblasts are attached to the flask, while myocytes remain in the supernatant. Cells are counted, diluted to appropriate concentration with DMEM supplemented with 10% FBS, antibiotics, 1x ITS and 0.1 mM BrdU, necessary to inhibit cell proliferation. Cells are plated at a concentration of 5 x 10^5 cells/ml, resulting in 80-90% confluence, and are cultured for 24 hours in a 5% CO_2 incubator at 37˚C prior to the experiments.

4.6 Fluorescence microscopy

Experiments involving microscopy were performed using an inverted microscope (Olympus IMT-2) equipped with a xenon lamp as a fluorescence light (75W), a 12 bit CCD camera provided with a cooling system (Miromax, Princeton Instruments), a 40x 1,3 NA oil objective and appropriate excitation and emission filters.

4.6.1 Measurement of ROS production in situ

ROS production in intact cells was measured using the Mitotracker Red fluorophore (MTR, Molecular Probes, λ_{ec} = 554 nm, λ_{em} = 576 nm). The probe is a rosamine derivative that accumulates selectively in the mitochondria due to the difference in potential present at the level of inner mitochondrial membrane. MTR presents a chloromethyl moiety that can bind to the thiol groups present at the level of mitochondrial proteins and be retained in these organelles. Production of ROS at mitochondrial level was determined measuring the increase in fluorescence intensity due to the formation of the fluorescent oxidized product of MTR following the increase in oxidative stress (Fig. 9).

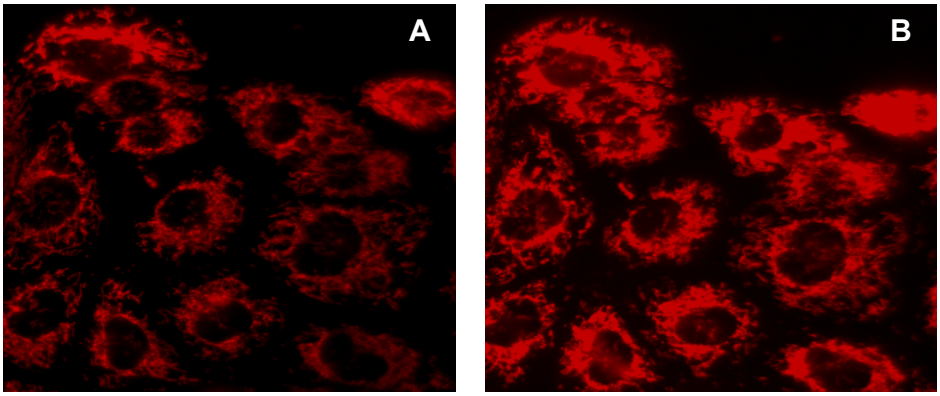

Figure 9. Fluorescence images showing HL-1 cardiomyocytes loaded with MTR: the effect of oxidative stress . HL-1 cardiomyocytes were loaded with 25 nM MTR and visualized by fluorescence microscopy. Images were acquired at the beginning of the experiment (panel A) and 30 minutes after the administration of 100 mM H_2O_2 (panel B).

At the moment of the experiments, cells were incubated for 15 minutes at 37°C with 25 nM MTR in HBSS. Following the incubation, cells were washed twice with HBSS. When MAO inhibitors were used, clorgyline, pargyline or selegiline were incubated for 15 minutes at 37°C and during the loading with MTR.

4.6.2 Determination of oxidative stress by DHE staining

LV tissue was cryosectioned to 10 micron thick slices using a LEICA CM 1850 microtome, termostated at -24°C. Sections were attached to polylysine precoated slides and dried to prepare them for further analysis.

ROS production was determined measuring variations in fluorescence intensity of the probe dihydroethidium (DHE). Once inside the cell, this probe can be oxidized by ROS to the fluorescent compound ethidium and irreversibly bind to nuclear DNA, a process that results in a further increase in fluorescence.

DHE (Sigma) was prepared as a 1 mM stock solution in DMSO and then diluted to a final concentration of 5 µM in degassed PBS. Considering that the solution is photosensible, all the operations were carried out in dark. The slides and the cryosections previously prepared were covered with a sufficient amount of DHE solution and incubated for 30 minutes at 37°C in humid atmosphere.

Afterwards, slides were washed in PBS to remove excess DHE solution (to reduce the background fluorescence). Slides were mounted with a 90% glycerol solution and covered with a cover slide. Slides were examined using a fluorescence microscope and a 20x air objective at 568 nm and 585 nm excitation and emission wavelengths respectively.

4.6.3 Image analysis

Images were analyzed using the Metamorph imaging software. Regions of interest were defined as regions rich in mitochondria and the fluorescence in these regions was monitored for the whole duration of the experiments. Variations of fluorescence intensities were analyzed and reported as mean of the variations in all regions analyzed. Considering that initial fluorescence intensities may be different in various regions that were considered, mean fluorescence was reported as percentage compared to the initial value.

4.7 Determination of cell viability

For determination of cell viability, the resazurin based assay was used. Resazurin is a redox indicator dye that can be added directly to cells in culture. Cells convert the dark blue oxidized form of the dye (resazurin) into a red reduced form (resorufin). This system is specific for viable cells since nonviable cells rapidly lose metabolic capacity and are not able to reduce resazurin. Results can be recorded with a spectrophotometer at 540 and 620 nm wavelengths to quantify the amount of reduced and oxidized form respectively. By calculating the ratio between the two values, it is possible to extract the number of viable cells in respect to the number of cells plated initially. This value has been normalized to the one obtained from control cells treated in the same conditions.

Cells were plated in 96 well plates at a density of 20 000 cell/well, 24 hours prior to the experiment. The medium was aspirated, cells added with 100 µl HBSS with 100 µM H_2O_2 or 5 µM arachidonic acid and incubated for various times, for 0.5 to 8 hours. At the end of each experiment, HBSS was aspirated and another

100 µl of culture medium was added containing 10% resazurin. Absorbance was recorded at the beginning and after 3 hours of incubation.

4.8 Silencing of MAO-A

HL-1 cardiomyocytes were plated in sterile 6 well plates containing sterile 24 mm diameter glass cover slide coated with fibronectin and gelatin. Cells were grown for 24 hours and when they reached around 30% confluence, cells were washed with sterile PBS to eliminate the antibiotics and added with Claycomb medium without antibiotics and norepinephrine. In separate tubes, transfection mixture was prepared and incubated for 5 minutes at room temperature, containing Opti-MEM I (Invitrogen), saline medium without FCS, and 1 µl/ml Lipofectamine 2000 (Invitrogen), transfecting reagent composed of lipid polycathions. siRNA solution containing a short RNA sequence complementary to a specific region of MAO-A mRNA was diluted in Opti-MEM I to a concentration of 50 nM and added to the mixture containing diluted Lipofectamine 2000. The sequence for MAO-A silencing was as follows: 3' GGAUCUAGGCAUAGAGACCUAUAAA 5'. Following incubation for 20 minutes at room temperature, necessary for the formation of complexes between siRNA and Lipofectamine, this mixture was added to each well containing cells and distributed homogeneously. Cells were incubated at 37°C in an atmosphere with 5% CO_2 for 48 hours. Transfection efficiency was assessed using a fluorescent indicator BLOCK-iT Fluorescent Oligo (Invitrogen), a dsRNA oligonucleotide marked with fluorescein-5-isothiocynate (FITC) and silencing efficiency was determined by Western blot.

4.9 Transverse aortic constriction (TAC)

Male C57Bl6 mice (Jackson Laboratories) at 9-11 weeks of age were used for the in vivo experiments. Pressure overload was induced by constricting transverse aorta. Anesthesia is induced with etomidate (0.5 ml/i.p.) and after intubation with a 16G plastic tube, anesthesia is maintained by 2% isoflurane gas supplemented by 95/5% O_2/CO_2. Mice are placed on a volume ventilator (120

breaths/min, 1.2 ml/g/min). Aorta was approached via minimal sternal incision and a 7-0 ligature was placed around the transverse aorta using a 27G needle to ensure consistent occlusion. This results in a 65-70% constriction after removal of the needle. The chest is closed using a 6-0 silk suture and negative pressure is the thorax restored by air evacuation using a PE-50 chest tube attached to a syringe. The skin is then closed with 5-0 silk and animals extubated and allowed to fully recover. Sham-operated mice undergo the same operation except that after the aortic arch is isolated, there is no ligature placed.

4.10 Chronic *in vivo* treatment with clorgyline

1 mg/kg clorgyline (Sigma) was administered by daily intraperitoneal injection using saline as a vehicle. Clorgyline stock solution at a concentration of 1 mg/ml was prepared in sterile physiological solution and consequently diluted to achieve the necessary concentration based on mice body weight. A volume of 150 μl was injected in each mouse. TAC mice not treated with clorgyline were subjected to the same protocol, except that they were injected with the vehicle.

4.11 Echocardiography

Trans-thoracic echocardiography was performed in conscious mice using a Hewlett-Packard Sono 5500 ultrasound and a Sequoia C256 (Siemens Corps, Mountain View, Calif) equipped with the 15MHz linear-array transducer. The heart was imaged in the 2D mode in the parasternal long-axis view with a depth setting of 2 cm. From this view, an M-mode cursor was positioned perpendicular to the interventricular septum and posterior wall of the left ventricle at the level of the papillary muscles. An M-mode image was obtained at a sweep speed of 100 mm/s. Diastolic and systolic left ventricle wall thickness, left ventricle end-diastolic (LVEDD) and end-systolic chamber dimensions (LVESD) were measured. All measurements were done from leading edge to leading edge. Average of 3 measurements was taken for the analysis. The percentage of LV fractional shortening (FS) and ejection fraction (EF) were calculated according to the following equations:

$$FS = [(LVEDD - LVESD)/LVEDD] \times 100$$

$$EF = [\{(LVEDD)^3 - (LVESD)^3\}/ (LVEDD)^3] \times 100.$$

LV mass was calculated according to uncorrected cube assumptions with some modifications using the equation:

$$LV\ mass\ (mg) = 1.055 \times [(LVEDD + LVPW + IVS)^3 - (LVEDD)^3],$$

where 1.055 is the gravity of myocardium, PWTD is diastolic posterior left ventricle wall thickness, and IVS is diastolic interventricular septal thickness.

4.12 PCR and real time RT-PCR

4.12.1 RNA extraction

Total RNA extraction from neonatal rat cardiomyocyte was performed using TRIzol reagent (Invitrogen), a monophasic solution of phenol and guanidine isothiocyanate, according to the manufacturer instruction. Briefly, cells were lysed directly in the 3.5 mm culture dish by adding 1 ml of TRIzol and passing the lysate several times through a pipette. The homogenized samples were incubated for 5 minutes at room temperature to permit the complete dissociation of nucleoprotein complexes. Then, 0.2 ml of chloroform were added, tubes shaken vigorously for 15 seconds and incubated at room temperature for 3 minutes. Samples were centrifuged at 12,000 × *g* for 15 minutes at 4°C. Following centrifugation, the mixture separated into a lower red, phenol-chloroform phase, an interphase, and a colorless upper aqueous phase which contained RNA. Aqueous phase was transferred into a new tube and RNA precipitated by the addition of 0.5 ml of isopropyl alcohol. Following 10 minutes incubation at room temperature, samples were centrifuged again at 12,000 × *g* for 15 minutes at 4°C and supernatant was discarded. RNA precipitate was washed with 70% ethanol,

briefly air dried and dissolved in 40 µl RNase free DEPC (diethylpyrocarbonate) treated water (Amersham).

RNA extraction from LV tissue was performed using RNeasy RNA extraction kit (Qiagen) according to the manufacturer's instructions. This technology combines the selective binding properties of a silica-based membrane with the speed of microspin technology. 30 mg of LV tissue were first lysed and homogenized in the presence of a highly denaturing guanidine-thiocyanate–containing buffer, which immediately inactivates RNases to ensure purification of intact RNA. Ethanol was added to provide appropriate binding conditions, and the sample was then applied to an RNeasy Mini spin column, where the total RNA binds to the membrane and contaminants are efficiently washed away. High-quality RNA was then eluted in 40 µl of DEPC treated water.

An aliquot was diluted in water and the absorbance of the solution was measured spectrophotometrically at 260 and 280 nm to determine the purity and the concentration of isolated RNA. Preparations with the ratio A_{260}/A_{280} higher than 1.8 were considered for further analysis.

4.12.2 cDNA synthesis

Reverse transcription reactions were performed using 1 to 5 µg of total RNA pretreated with DNAse I (Invitrogen), to eliminate the contaminating DNA. After addition of dNTP and oligo dT to prime the first strand cDNA synthesis, RNA was denatured at 65°C for 5 minutes and then placed on ice. Superscript II (Invitrogen) was the added and the mixture incubated at 42˚C for 50 minutes and 70˚C for 15 minutes to synthesize cDNA.

4.12.3 PCR

Each PCR reaction was performed in a 20 µl volume combining 2 µl of cDNA, 0.25 µM of forward e reverse primers, 200 µM of each dNTP (dATP, dTTP, dGTP, dCTP Amersham Pharmacia), 2 mM $MgCl_2$, 0.025U/µl Taq polimerase (HotGoldstar Applied Biosystem) in a 10X buffer (150 mM TRIS/HCl

pH 8, 500 mM KCl, 0.1% v/v Tween 20). Applied Biosystems thermal cycler was used (GeneAmp 9700).

Following are the amplification cycling conditions:

- Initial step 95°C for 9 minutes
- Denature 95°C for 45 seconds
  Anneal 64°C for 30 seconds 35 cycles
  Extend 72°C for 30 seconds
- Complete the amplicons 72°C for 3 minutes
- Final step 4°C.

The sequence of forward e reverse primers used for MAO-A and MAO-B are as follows:

MAO-A F 5'-AAGCAAGACATGCTGAGGAATG-3'

MAO-A R 5'-GGTGACTGAGAATATCCGAGAGG-3'

Amplicon size: 200 bp. Anneal temperature: 64°C.

MAO-B F 5'-CGCTCTTTGTGAACCTGTGTG-3'

MAO-B R 5'-CCTGTCTGGTCAATGTGGATCA-3'

Amplicon size: 230 bp. Anneal temperature: 64°C.

To visualize the PCR products, amplified DNA was run on agarose gel in the presence of ethidium bromide. Briefly, loading buffer was added to the samples which were loaded on a 2% agarose gel in 1X TAE buffer (40mM Tris/acetate, 1mM EDTA), in the presence of 0.25 µg/ml ethidium bromide. Gel was immersed in running buffer (TAE 1X) and subjected to an electric field of 135 V for 20 minutes. The bands were visualized with the fluorescence reader DC290 (Kodak) and the image was analyzed using the KODAK 1D software.

4.12.4 Real time PCR

Each PCR reaction was performed in a 20 µl volume combining 50 ng of cDNA, 0.25 µM of forward e reverse primers and 10 µl of 2X Sybr green Master mix (Applied Biosystems). Applied Biosystems thermal cycler was used (GeneAmp 9700).

Following were the amplification cycling conditions:

- Initial step 95°C for 10 minutes
- Denature 95°C for 15 seconds
  Anneal 60°C for 1 minute 40 cycles
  Extend 72°C for 30 seconds
- Dissociation stage 95°C for 15 seconds
  60°C for 15 seconds
  95°C for 15 seconds

Primer sets for the specific target genes were designed to span one or more introns. The sequences of forward and reverse primers used for each gene that was investigated are shown in Table 1.

Target gene	Primer sequence
rat BNP	F 5' ATGCAGAAGCTGCTGGAGCTGATA 3' R 5' CTTCTGCCCAAAGCAGCTTGAACT 3'
rat MAO-A	F 5' ACACTTTCTCCTCCTTGTGTGGGT 3' R 5' AGCATAGGCACTTGAGAGGCATGA 3'
mouse MAO-A	F 5' AGGTGGCTCTGGCCAAATAAGTGA 3' R 5' ACCGGTGGGATGGCACTAATTACA 3'
rat NFAT3	F 5' ATGGTGGCTACAGCCAGCTATGAA 3' R 5' CACAGTCAATGTTGGCAGCCATGT 3'
rat NFAT4	F 5' TCAGCAAGTATCGACTGTGCAGGT 3' R 5' TCGCTGAGAGCACTCAACAGGAAT 3'
mouse ANP	F 5' GCTTCCAGGCCATATTGGAGCAAA 3' R 5' TGACCTCATCTTCTACCGGCATCT 3'
rat GAPDH	F 5' GACATGCCGCCTGGAGAAAC 3' R 5' AGCCCAGGATGCCCTTTAGT 3'
mouse GAPDH	F 5' CATGGCCTTCCGTGTTCCTA 3' R 5' CCTGCTTCACCACCTTCTTGAT 3'

Table 1. Sequences of the primers used for real time PCR.

The specificity of the primers was assessed examining the dissociation curves for each PCR product.

Standard curves were run in parallel and their slopes and y-intercept were used for data analysis. All the samples were normalized to the expression of GAPDH gene, taken as a reference to ensure equal loading.

4.13 Protein analysis by gel electrophoresis (Western blot)

4.13.1 Samples preparation

Samples were prepared from previously snap frozen LV tissue stored at -80C. 50 mg of tissue was homogenized in 1 ml of lysis buffer (Cell signaling) using Polytron homogenizer. The composition of the lysis buffer was:

20 mM Tris-HCl (pH 7.5)

150 mM NaCl

1 mM Na_2EDTA

1 mM EGTA

1% Triton

1mM PMSF

1X protease inhibitor mix (Sigma)

1X phosphatase inhibitor mix (Sigma)

Homogenized samples were then centrifuged at 13 000 x g for 10 minutes at 4°C and the pellet was discarded. Protein concentration was determined in the supernatant by biuret method as described previously. To denature and solubilize the proteins, Nupage sample buffer (564 mM Tris base, 8% LDS (lithium dodecyl sulphate), 40% glycerol, 2.04 mM EDTA, 0.88 mM SERVA® Blue G250 and 0.7 mM Phenol Red, 5% β-mercaptoethanol, pH 8.5) was then added and samples were boiled at 100°C for 10 minutes. Then they were loaded on the gel or aliquoted and stored at -20°C.

4.13.2 SDS-polyacrylamide gel electrophoresis (SDS-PAGE) and immunoblot

Electrophoresis was performed on polyacrylamide gel [149], at a 12% concentration in the *separating* gel and 5% concentration in the *stacking* gel, prepared in glass slabs 1 mm thick. Following solutions were used for the preparation of the gel:

- Acrylamide/bisacrylamide: 30% acrylamide and 0.8% bisacrylamide
- Lower Tris-HCl (4x): 1.5 M Tris-HCl and 0.4% SDS, pH 8.8
- Upper Tris-HCl (4x): 0.5 M Tris-HCl and 0.4% SDS, pH 6.8

- Running buffer (4x): 0.1 M Tris-HCl, 0.77 M Glycine and 0.4% SDS, pH 8.3

The polymerization of the gel was obtained by the addition of TEMED (Pharmacia) and APS (0.1mg/ml) (Amersham Biosciences).
Samples were run on the gel at room temperature using the Electrophoresis Power Supply ST504D (Apelex) which provided a constant voltage of 150V in the stacking gel and 200V in the separating gel.

In order to make the proteins accessible to antibody detection, they were moved from within the gel onto a nitrocellulose membrane. Immunoblotting was performed according to Towbin[150]. Once the samples finished the run, the gel was washed from the excess SDS with the transfer buffer (25 mM Tris, 192 mM glycine, 10% methanol, pH 8.0). A 0.45 micron nitrocellulose membrane (Bio-Rad Laboratories) was placed on top of the gel, avoiding creating bubbles, and a stack of tissue papers placed on top. This stack was then inserted into a transfer box filled with transfer buffer, so that the gel is oriented towards the cathode and the membrane towards the anode. When a current is applied to the electrodes, this causes the proteins to migrate from the negatively charged cathode to the positively charged anode, i.e. towards the membrane. The best efficiency of transfer was observed when a 150 mA current was applied (Hoefer EPS2A200) overnight at 4°C.

Once the transfer was carried out, the membrane was saturated using a blocking solution composed of 50 mM Tris-HCl, 2 mM $CaCl_2$, 85 mM NaCl, 3% BSA, pH 8.0, for 1 hour at room temperature.

The antibodies used for the proteins of interest were diluted in the blocking solution. The folowing primary antibodies were used:

Anti MAO A (Santa Cruz), dilution 1:1000
Anti β-actin (Abcam), dilution 1:2000
Anti phospho-Akt (Cell Signaling Technologies), dilution 1:1000
Anti Akt (Cell Signaling Technologies), dilution 1:1000
Anti caspase-3 (Cell Signaling Technologies), dilution 1:1000
Anti GAPDH (Cell Signaling Technologies), dilution 1:2000

All the primary antibody incubations were carried out overnight at 4°C. Following the incubation, membranes were washed three times with the washing buffer composed of 50 mM Tris-HCl, 85mM NaCl, 0.1% Tween 20, pH 7.4 (10 minutes each wash). Secondary antibodies were diluted in blocking solution and incubated with the membrane for 1 hour at room temperature. Secondary antibodies used were:

Anti mouse (Pierce), dilution 1:2000
Anti rabbit (Pierce), dilution 1:2000

Secondary antibody in conjugated to a reporter enzyme, namely horseradish peroxidase (HRP). When in the presence of a chemiluminescent agent, they can interact and the reaction product produces luminescence in proportion to the amount of protein.
Prior to the detection, membrane was washed three times (15 minutes each wash).

4.13.3 Chemiluminescent detection

Membrane was exposed to SuperSignal West Pico or Femto Chemiluminescent Substrate (Pierce) for 1 minute. This incubation causes the generation of luminous signal due to the oxidation of the substrate by HRP bound to the secondary antibody. The light, emitted at λ_{max}340 nm, was detected by a CCD camera (Image Station 440 CF, Kodak).

4.13.4 Densitometry

Images of the western blot acquired were analyzed using the ImageJ software (NIH). This program allows the quantification of the optical density of the bands that are directly proportional to the protein content.

4.14 Statistical analysis

Comparisons between two groups were performed by Student's t-test. Comparisons between multiple groups were performed by two-way ANOVA followed by a Tukey's multiple comparison test. A value of $p<0.05$ was considered significant.

5 RESULTS AND DISCUSSION

5.1 The role of MAO in the oxidative stress

5.1.1 MAO expression at cardiac level

Up to date, MAO have been extensively studied at the level of central nervous system while less attention has been given to their distribution and role in the peripheral tissues. Some evidence exists regarding MAO distribution in the heart, where MAO-A is the isoform prevalently present and located within the cardiomyocytes. To confirm this pattern of expression in our model, we initially determined the expression level of MAO-A and B in the cardiac tissue. The mRNA expression of MAO-A and B was determined by RT-PCR. As shown in Fig. 10, cardiac cells and tissue express prevalently MAO-A isoform, while MAO B expression level is almost negligible.

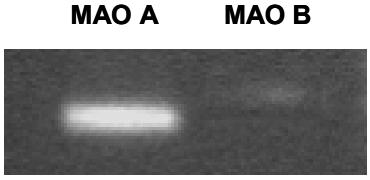

Figure 10. Expression levels of MAO-A and –B mRNA in mouse heart. Total RNA was extracted and reverse transcribed as described in Materials and Methods. Equal amounts of cDNA were amplified by PCR using specific primers and each PCR product showed a single band. DNA was visualized on agarose gel in the presence of ethidium bromide. The amplicon size for MAO-A product was 200 bp and for MAO-B 230 bp.

However, the gene expression level does not necessarily reflect the levels of protein expression or enzyme activity. This is due to a series of post-transcriptional control processes that occur in cells and that might enhance or lessen the translation of the synthesized mRNA. Therefore, in the absence of specific antibodies necessary to distinguish between each isoform, we confirmed these results measuring the activity of these enzymes in mitochondria isolated from mouse heart. MAO-A and B activities were determined measuring the

production of H_2O_2 by means of Amplex Red, which is oxidized to resorufin in the presence of H_2O_2. Mitochondria were incubated with 100 μM tyramine, substrate for MAO-A and B, and serotonin (5-HT), substrate only for MAO A, in the presence or in the absence of specific MAO inhibitors. There was a marked increase in H_2O_2 formation with both substrates and preincubation of mitochondria with clorgyline, a specific MAO-A inhibitor, or pargyline, an inhibitor of both isoforms, completely prevented H_2O_2 production (Fig. 11). However, MAO-B inhibitor selegiline did not influence H_2O_2 formation suggesting that this isoform was not involved in tyramine or serotonin catabolism. Taken together, these data strongly support the notion that MAO-A is indeed the prevalent isoform present at the level of cardiomyocytes.

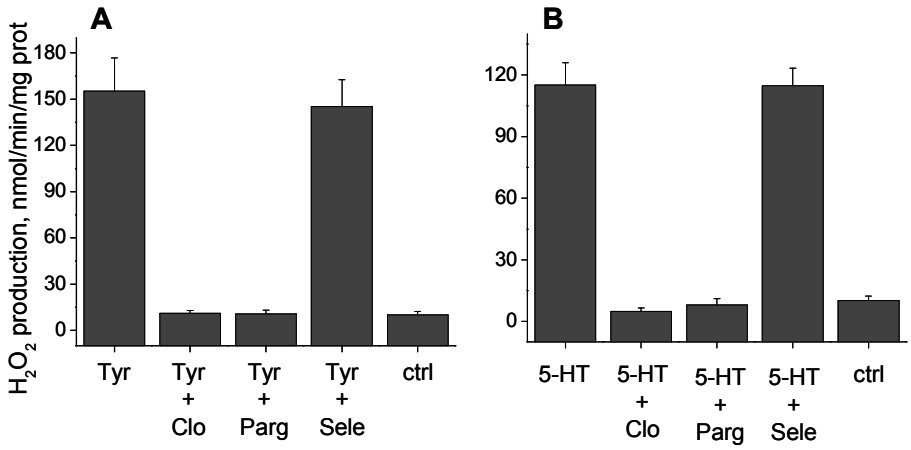

Figure 11. Effect of selective MAO inhibitors on MAO activity in isolated heart mitochondria. Mitochondria (0.5 mg/ml) were incubated with 10 μM Amplex Red and 15 μg/ml HRP in the standard medium for a total volume of 2 ml. The reaction was started by the addition of 100 μM MAO substrates tyramine (Tyr, panel A) or serotonin (5-HT, panel B). Clorgyline (Clo, 100 nM), pargyline (Parg, 100 μM) or selegiline (Sele, 50 μM) were preincubated with mitochondrial proteins for 2 minutes before the start of the experiment. All the experiments were performed at pH 7.4 and at 37°C.

5.1.2 Investigation of the effects of MAO inhibitors on mitochondrial function

MAO inhibition has been reported to protect cardiomyocytes against the deleterious effects of serotonin[37]. Data available in the literature, as well as data previously obtained in Prof. Di Lisa's laboratory, show that MAO inhibition is able to prevent cardiac ischemia/reperfusion injury by reducing the oxidative stress. Mitochondria, and in particular mitochondrial respiratory chain, are

considered one of the major sources of ROS. Considering that administration of MAO-A inhibitor clorgyline at early reperfusion is able to prevent structural and functional changes of the myocardium following ischemia/reperfusion injury, this would suggest that MAO are actually a major source of ROS in the mitochondria and respiratory chain could likely represent a target rather than a source of ROS. However, to exclude the possibility that MAO inhibitors could affect other cellular processes involved in myocardial injury, such as mitochondrial function, we assessed their specificity in isolated heart mitochondria.

Initially, using a Clark electrode we evaluated whether MAO inhibitors could affect mitochondrial respiration. Mitochondria, energized with glutamate and malate, were incubated with increasing concentrations of pargyline and selegiline (0-1 mM) and oxygen consumption was measured in basal state (state 4), which reflects the minimal electron flux necessary to compensate for the inner mitochondrial membrane passive permeability to protons, and in the uncoupled state, representing the maximal respiration induced by the addition of protonophore FCCP. Figure 12 shows that both inhibitors had no effect on mitochondrial oxygen consumption in basal or uncoupled state.

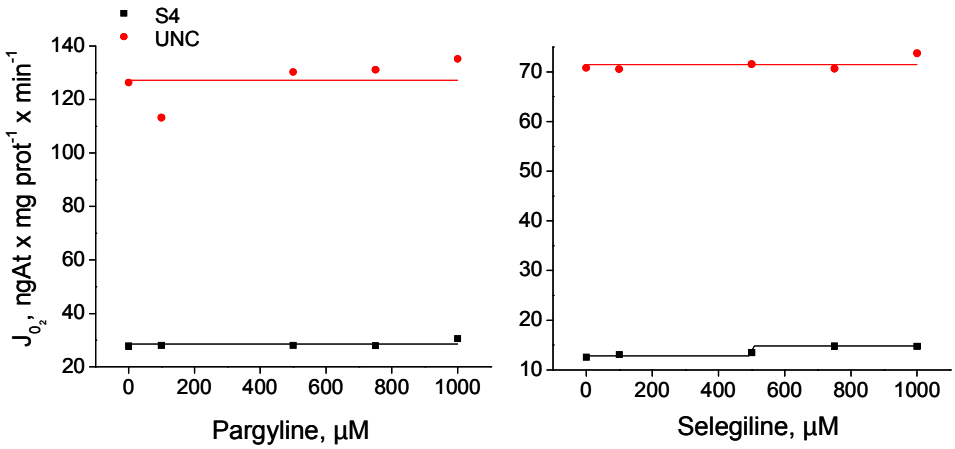

Figure 12. Effect of selective MAO inhibitors on mitochondrial oxygen consumption. Mitochondria (0.5 mg/ml) were incubated with 5/2.5 mM glutamate/malate as substrates in the standard medium for a total volume of 2 ml. One minute after the addition of mitochondria, pargyline (panel A) or selegiline (panel B) were added at indicated concentrations and oxygen consumption at state 4 (S4) was monitored for 3 minutes. The addition of 100 nM FCCP followed and the maximal respiration was measured for another 3 minutes (UNC). All the experiments were performed at pH 7.4 and at 37°C.

Different results were obtained with clorgyline. As shown in Figure 13 panel A, in the presence of glutamate and malate as substrates, which provide the reducing equivalents at the level of complex I of the respiratory chain, clorgyline had no effect on basal respiration at concentrations from 0-100 μM. Conversely, clorgyline inhibited FCCP-stimulated respiration at concentrations higher than 50 μM. In mitochondria energized with succinate, substrate that provides reducing equivalents at the level of complex II, clorgyline did not affect oxygen consumption, either at basal or uncoupled state (Fig. 13, panel B). These results suggest that clorgyline might interact with the flavinic portion of Complex I of the respiratory chain, one of the major sources of ROS. However, it should be mentioned that the observed effect is nonspecific, since it occurs only at concentrations much higher than those required for MAO inhibition. Indeed, the inhibition of the respiratory chain occurs only at concentrations higher than 50 μM, while MAO inhibition occurs at concentration as low as 100 nM.

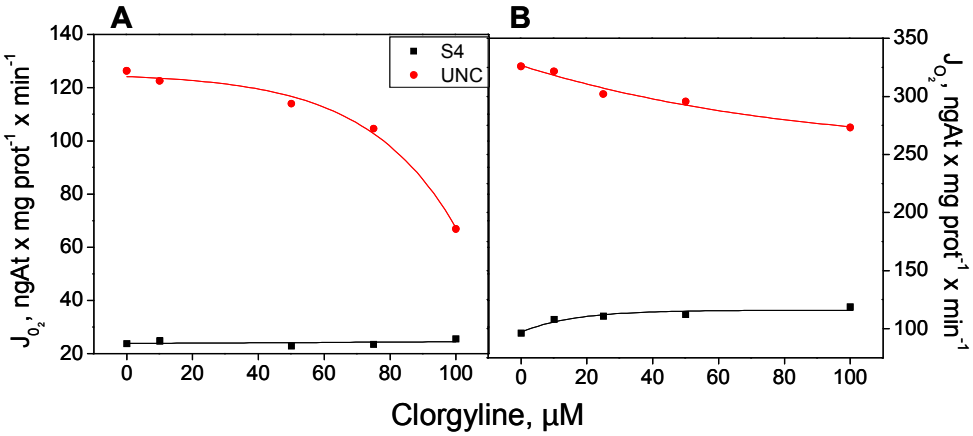

Figure 13. Effect of clorgyline on mitochondrial oxygen consumption. Mitochondria (0.5 mg/ml) were incubated in the standard medium for a total volume of 2 ml with 5/2.5 mM glutamate/malate (panel A) or 5 mM succinate in the presence of 2 μM rotenone (panel B) as substrates. One minute after the addition of mitochondria, clorgyline was added at indicated concentrations and the oxygen consumption at state 4 (S4) was monitored for 3 minutes. The addition of 100 nM FCCP followed and the maximal respiration was measured for another 3 minutes (UNC). All the experiments were performed at pH 7.4 and at 37°C.

We also tested whether clorgyline was able to influence the ROS production by respiratory chain. To this aim, H_2O_2 production was induced incubating mitochondria with succinate in the absence of rotenone, a condition that results in increased ROS production at the level of complex I due to retrograde electron flux. Clorgyline (1 μM) did not influence ROS production, as determined by Amplex Red fluorescence. Another important site of ROS formation is at the level of complex III of the respiratory chain. Indeed, inhibition of complex III with Antimycin A determines an escape of electrons and partial oxygen reduction resulting in increased ROS formation. As shown in Figure 14, clorgyline did not have any effect on the rate of H_2O_2 formation, confirming its specific action at low concentrations which are highly effective in inhibiting MAO.

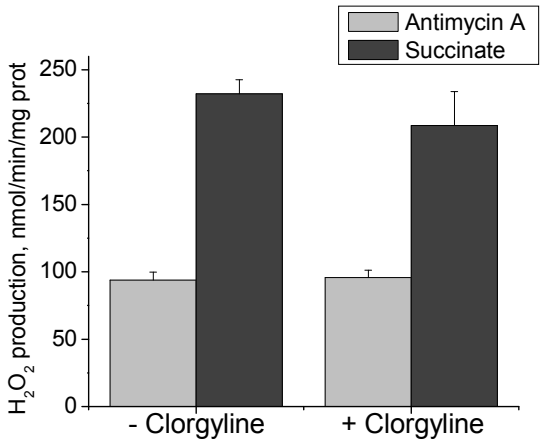

Figure 14. Effect of clorgyline on H_2O_2 production by the respiratory chain. Mitochondria (0.5 mg/ml) were incubated in the standard medium with 10 μM Amplex Red and 15 μg/ml HRP for a total volume of 2 ml. The reaction was started after the addition of Antimycin A 1 γ or 5 mM succinate and monitored for 10 minutes. When present, 1 μM clorgyline was preincubated for 2 minutes before the experiments. All the experiments were performed at pH 7.4 and at 37°C.

5.1.3 Effect of pharmacological inhibition of MAO on oxidative stress induced by H_2O_2

We have started our investigation on MAO involvement in the oxidative stress evaluating whether MAO inhibition could reduce or prevent ROS generation induced by agents such as H_2O_2. To this aim, HL-1 cardiomyoctes

were used, a murine cell line that displays the majority of the physiological characteristics of adult cardiomyocytes, such as electrophysiological profile, cytoplasmatic organization and myofibrillar genesis[151]. ROS production at mitochondrial level was determined by means of Mitotracker Red (MTR). MTR is a reduced derivative of rosamine that can accumulate in mitochondria due to the difference in membrane potential present at the level of inner mitochondrial membrane and, for the presence of the chloromethyl moiety, it can associate with the mitochondrial proteins and remain sequestered in these organelles. The reduced probe does not fluoresce until it enters an actively respiring cell, where it is oxidized to the corresponding fluorescent mitochondrion-selective probe and then sequestered in the mitochondria. Following an increase in ROS production, MTR is oxidized with a parallel increase in fluorescence, directly proportional to the increase in oxidative stress.

Depending on concentrations, H_2O_2 is known to mediate intracellular signaling leading to, for example, cell proliferation or cell death [143]. To investigate the role of MAO in the oxidative stress induced by H_2O_2 independently of its effect on cell viability, we initially established experimental conditions that do not result in loss of viable cells. Cell viability was determined using resazurin, a redox indicator dye that is reduced to resorufin by metabolically active cells. The product of this reaction can be measured spectrophotometrically at 540 and 620 nm, to determine the amount of reduced and oxidized dye, respectively. Therefore, we initially determined whether 100 μM H_2O_2 was able to affect cell viability.

Figure 15 shows that there was no change in cell viability up to two hours following incubation with 100 μM H_2O_2. However, after prolonged incubation, H_2O_2 was able to induce a significant degree of cell death.

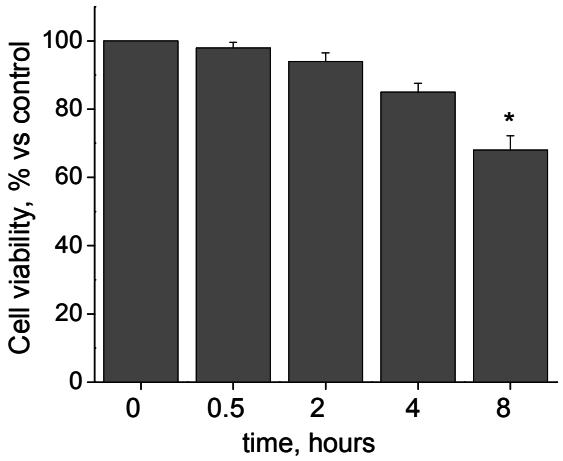

Figure 15. Effect of H_2O_2 on cell viability in HL-1 cardiomyocytes. Cells were incubated with 100 μM H_2O_2 for indicated times. At the end of the protocol, resazurin was added to the culture medium and cell viability was determined as indicated in Materials and Methods. *$p<0.001$ vs control*.

Next, we assessed levels of ROS production and possible involvement of MAO in this process. As shown in Figure 16, addition of 100 μM H_2O_2 to HL-1 cardiomyocytes resulted in a 50% increase in MTR fluorescence after 30 minutes of incubation compared to the control cells. To determine whether MAO activity could contribute to the instauration of the oxidative stress, selective MAO inhibitors were used. HL-1 cardiomyocytes were preincubated with clorgyline, a selective MAO-A inhibitor, selegiline, MAO-B inhibitor, or pargyline, inhibitor of both isoforms. Both clorgyline and pargyline were able to reduce by 60% the oxidative stress induced by the addition of H_2O_2. However, MAO-B inhibitor selegiline, showed no effect on ROS formation. These results suggest that MAO-A might play a major role in the oxidative stress induced by H_2O_2. MAO-B appears not to be involved, likely because it is not present at the cardiomyocyte level, as supported by the experiments performed in isolated heart mitochondria.

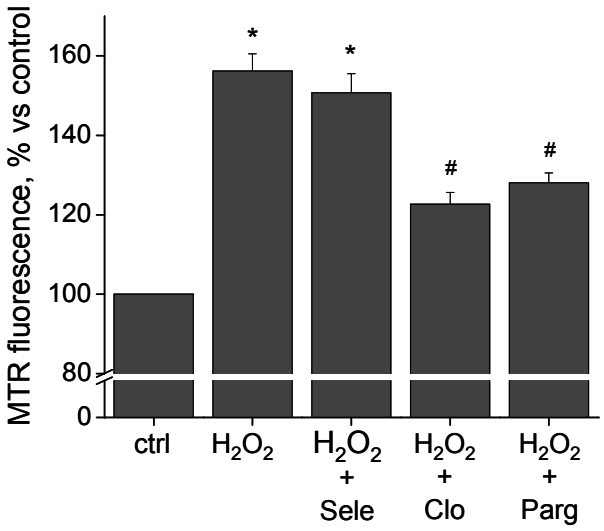

Figure 16. Effect of MAO inhibitors on oxidative stress induced by H_2O_2. Cells were incubated at 37°C with 25 nM MTR and then treated with 100 μM H_2O_2 for 30 minutes. When present, MAO inhibitors selegiline (Sele, 1 mM), clorgyline (Clo, 1 μM) or pargyline (Parg, 2 mM) were incubated with the cells for 30 minutes prior to the addition of H_2O_2. **p<0.05 vs control, #p<0.05 vs H2O2.*

5.1.4 Effect of pharmacological inhibition of MAO on oxidative stress induced by arachidonic acid

We also investigated whether a pro-apoptotic agent such as arachidonic acid was able to induce oxidative stress and whether this process involves MAO. Arachidonic acid is a potent inducer of mitochondrial permeability transition pore, a multiproteic channel present at the level of inner mitochondrial membrane. Opening of PTP causes a collapse in mitochondrial membrane potential ($\Delta\Psi_m$) and release of cytochrome c which has a determinant role in initiating the cascade of events leading to apoptosis[152].

We first determined the time-course in the occurrence of apoptosis following treatment with arachidonic acid and then we investigated whether this event was preceded by an increase in oxidative stress. As with H_2O_2, arachidonic acid also induced cell death after prolonged incubation (Fig.17).

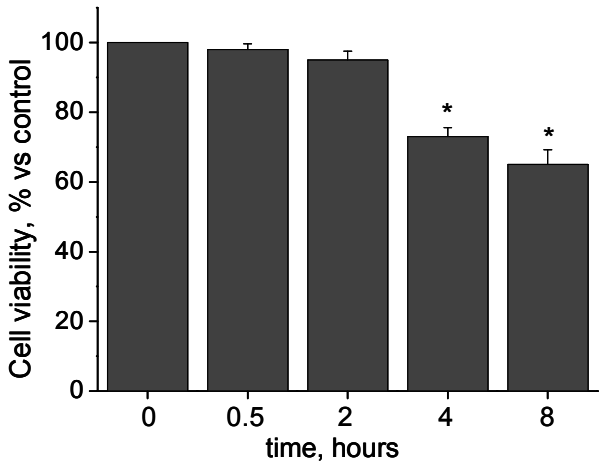

Figure 17. Effect of arachidonic acid on cell viability in HL-1 cardiomyocytes. Cells were incubated with 5 μM arachidonic acid for indicated times. At the end of the protocol, resazurin was added to the culture medium and cell viability was determined as indicated in Materials and Methods. **p<0.001 vs control.*

Treatment of HL-1 cardiomyocytes with 5 μM arachidonic acid determined an increase in MTR fluorescence within 15 minutes of administration (Fig. 18). To evaluate whether MAO could contribute to this event and which isoform might be involved, cells were preincubated with clorgyline, specific MAO-A inhibitor, and selegiline, MAO-B inhibitor. As shown in Figure 18, clorgyline completely prevented arachidonic acid induced oxidative stress. Conversely, when cells were pretreated with selegiline, the level of oxidative stress was unchanged compared to the untreated cells. Once again, these results support the hypothesis of a major involvement of MAO-A, but not MAO-B, in the oxidative stress.

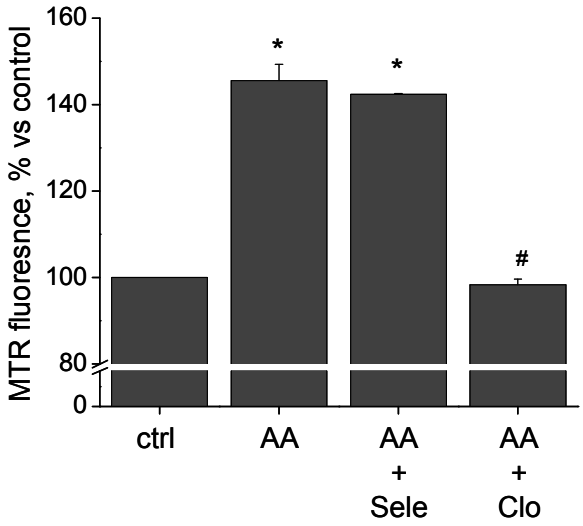

Figure 18. Effect of MAO inhibitors on oxidative stress induced by arachidonic acid. Cells were incubated at 37°C with 25 nM MTR and then treated with 5 μM arachidonic acid (AA) for 20 minutes. When present, MAO inhibitors selegiline (Sele, 1 mM) or clorgyline (Clo, 1 μM) were incubated with the cells for 30 minutes prior to the addition of arachidonic acid. *$*p<0.05$ vs control, $^{\#}p<0.05$ vs AA.*

5.1.5 Effect of genetic inhibition of MAO-A on oxidative stress: siRNA

The previous experiments suggest that MAO inhibition is able to decrease or completely prevent oxidative stress induced by exogenous stimuli and that MAO-A is the major isoform involved in this process. To rule out the possibility that nonspecific effects of the inhibitors used contribute to cardiomyocyte protection and to confirm the involvement of MAO-A, we decided to abolish the level of MAO-A expression by means of siRNA.

To this aim, short 25 bp sequences of RNA complementary to the specific region of MAO-A mRNA were designed. These oligoribonucleotides present proprietary modifications on the sense strand (Stealth RNAi). The increased length offers higher targeting specificity compared to the traditional siRNA. The proprietary modification on the sense strand ensures that only the anti-sense strand will be utilized by the RISC for gene targeting, while any potential off-target effect from the sense strand is totally eliminated. In addition to the targeting specificity, Stealth RNAi are also more stable in cull culture medium and provide a longer lasting knockdown effect in cells. The efficiency of the silencing depends on the specificity of the interaction between the RNAi and target mRNA which

should also present the pairing region well exposed for the RNAi to recognize it and interact. Transfection efficiency is directly proportional to the extent of silencing and therefore it was assessed using dsRNA, an oligonucleotide conjugated to FITC. Using 50 nM of siRNA and 1 μl/ml of Lipofectamine 2000 it was possible to obtain around 90% transfection efficiency (Fig. 19, panel A). As determined by Western Blot and shown in figure 19, after 48 hours of transfection MAO-A protein expression was reduced by 90% in siRNA treated cells.

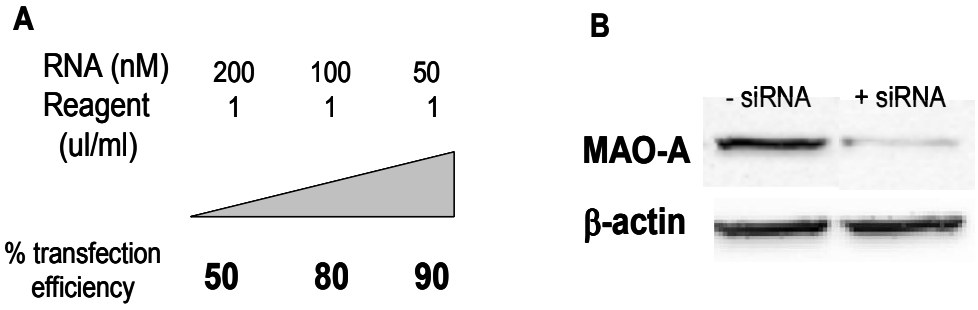

Figure 19. Silencing of MAO-A in HL-1 cardiomyocytes. Panel A: Transfection efficiency was determined varying the concentration of siRNA. After 48 hours of incubation with 50 nM siRNA and 1 μl/ml Lipofectamine 2000, protein content of MAO-A was determined by Western Blot (panel B).

siRNA treated cells were subjected to the same protocol as described previously. Control and siRNA treated cells were treated with 100 μM H_2O_2 and ROS production was determined measuring the fluorescence of MTR. Oxidative stress was reduced by 60% in siRNA treated cells as compared to control cells after treatment with H_2O_2 (Fig. 20). Remarkably, silencing of MAO-A provided the same extent of protection as the pharmacologic treatment with clorgyline. Furthermore, preincubation of siRNA treated cells with clorgyline did not provide any further protective effect.

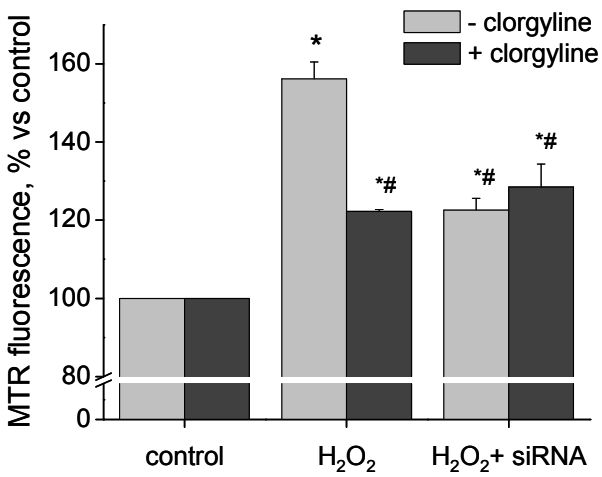

Figure 20. Effect of MAO-A silencing on oxidative stress induced by H_2O_2. 48 hours after the transfection cells were incubated at 37°C with 25 nM MTR and then treated with 100 μM H_2O_2 for 30 minutes. Clorgyline (1 μM) was incubated with the cells for 30 minutes prior to the addition of H_2O_2. *$^{*}p<0.05$ vs control, $^{\#}p<0.05$ vs H_2O_2.*

Cells were also transfected with a nonspecific RNA, differing from the siRNA for the presence of two different bases in its primary sequence. This was necessary to demonstrate that the observed effects were exclusively attributable to siRNA used to silence MAO-A expression and not to other nonspecific effects. Figure 21 shows the inability of the nonspecific oligonucleotide to reduce the H_2O_2-induced oxidative stress.

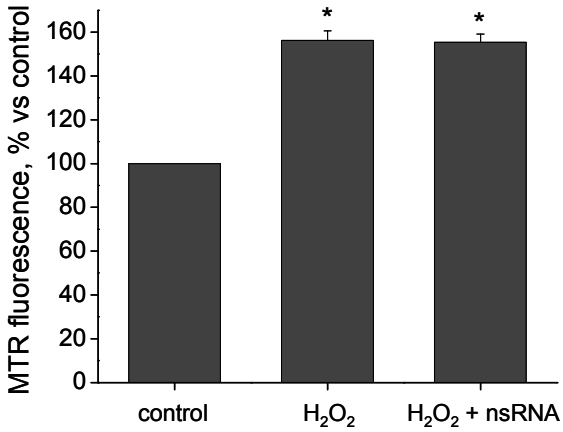

Figure 21. Effect of cell transfection with non specific RNA on oxidative stress induced by H_2O_2. 48 hours after the transfection with a non specific RNA (nsRNA), differing from the siRNA for the presence of two different bases in its primary sequence, cells were incubated at 37°C with 25 nM MTR and then treated with 100 μM H_2O_2 for 30 minutes. **p<0.05 vs control*.

Finally, it was evaluated whether silencing of MAO-A was also able to prevent the oxidative stress induced by arachidonic acid. As shown in Figure 22, ROS production was completely prevented in siRNA treated cells after the addition of 5 μM arachidonic acid. As previously, this effect was comparable to the effects observed with clorgyline and it was exclusively attributable to the silencing of MAO-A.

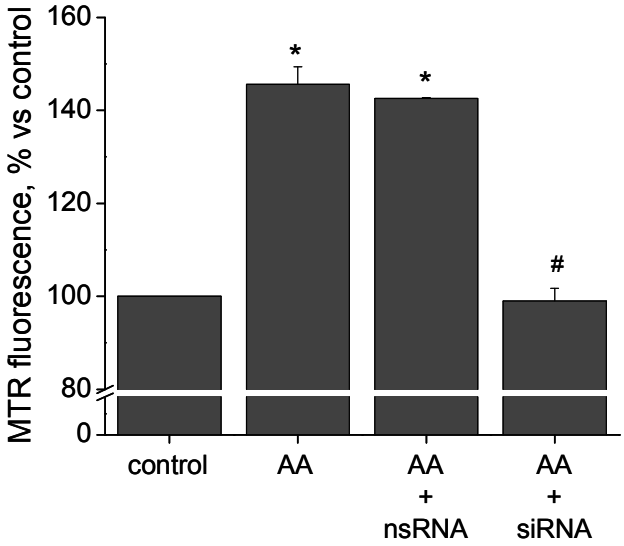

Figure 22. Effect of MAO-A silencing on oxidative stress induced by arachidonic acid. 48 hours after the transfection cells were incubated at 37°C with 25 nM MTR and then treated with 5 μM arachidonic acid (AA) for 20 minutes. To prove the specificity of siRNA, cells were also transfected with a non specific oligonucleotide (nsRNA). **p<0.05 vs control, #p<0.05 vs AA*.

5.2 Involvement of MAO-A in hypertrophy and heart failure

5.2.1 Investigation of MAO-A role in *in vitro* hypertrophy

Cardiac myocytes become terminally differentiated during the perinatal period and are incapable of undergoing complete cycles of cell division. However, cardiomyocytes possess the potential for adaptive growth achieved by the expansion of already existing cells (i.e. hypertrophy). Myocyte hypertrophy can occur in response to increased hemodynamic load caused by, for example, hypertension. Heart is also vulnerable to cellular stresses that promote myocyte death by necrosis or apoptosis. To compensate for the loss of contractile tissue, myocytes undergo hypertrophic growth to maintain cardiac function. Although this process provides initial compensation to the stress, sustained hypertrophic stimulation can become maladaptive and lead to heart failure. Oxidative stress is one of the key stresses that may contribute to cardiac remodeling and maladaptive hypertrophy and, up to date, a number of intracellular ROS sources have already been identified. Data provided here unequivocally demonstrate that MAO-A is involved and plays a major role in the oxidative stress at cardiomyocyte level. Since failing myocardium is subjected to increased oxidative burden and altered catecholamine cycling/turnover[153], we hypothesized that MAO-A might be involved in maladaptive hypertrophy.

Initially, we investigated whether a causative link exists between pro-hypertrophic stimuli and MAO-A. To this aim, neonatal rat cardiomyocytes were incubated with the α,β-adrenergic agonist NE (1 μM). This resulted in induction of hypertrophy after 24 hours, measured as increase in BNP expression, paralleled by a 3-fold up-regulation of MAO-A gene expression (Fig. 23, panels A and B).

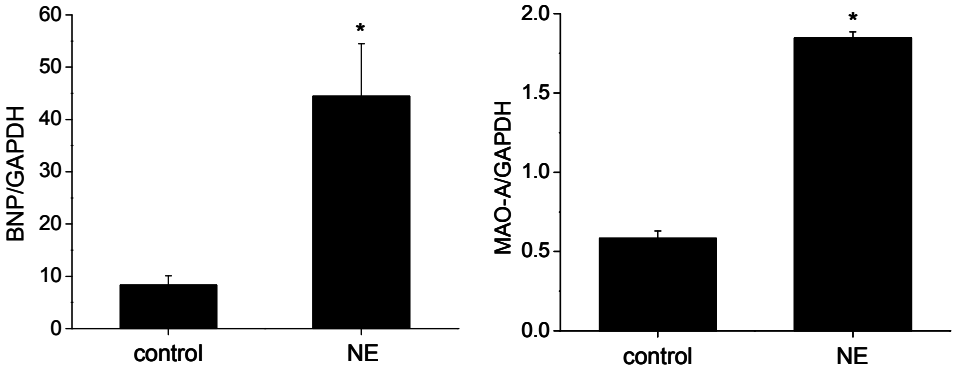

Figure 23. *In vitro* induced hypertrophy following incubation with norepinephrine. Neonatal rat cardiomyocytes were incubated with 1 μM norepinephrine (NE) for 24 hours at 37°C. RNA was extracted and reverse transcribed as described in Materials and Methods. Gene expression level of BNP (panel A) and MAO-A (panel B) were determined by real time RT-PCR using primers specific for those transcripts. GAPDH gene expression was used as internal control. **p<0.05 vs control*.

Furthermore, when myocytes were preincubated with 1 μM clorgyline, NE induced hypertrophy was partially reduced (Fig. 24), suggesting that this hormone is transported into the cell and degraded by MAO-A resulting in increased H_2O_2 production that can likely contribute to the development of hypertrophy.

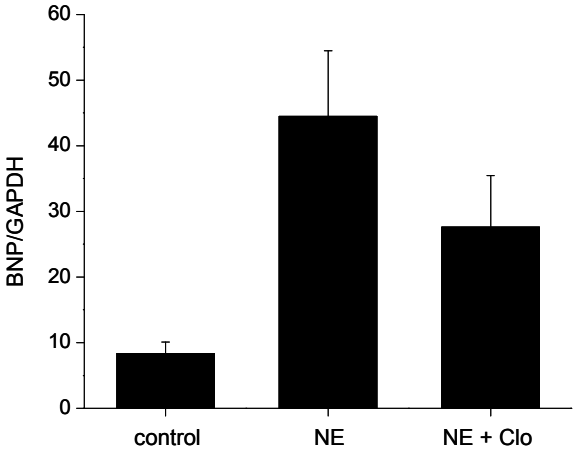

Figure 24. Effect of MAO-A inhibition on NE-induced induced hypertrophy in neonatal rat cardiomyocytes. Neonatal rat cardiomyocytes were incubated with 1 μM NE for 24 hours at 37°C. Cells were pretreated with 1 μM clorgyline (Clo) for 1 hour prior to the addition of NE and clorgyline was present in the culture medium for the whole duration of the experiment. RNA was extracted and reverse transcribed as described in Materials and Methods. Gene expression level of BNP was determined by real time RT-PCR using primers specific for this transcript. GAPDH gene expression was used as internal control.

This hypothesis was further corroborated by incubating myocytes with tyramine, a MAO substrate that does not interact with adrenergic receptors. As shown in Figure 25, tyramine induced an increase in ROS production at mitochondrial level and following 24 hours of incubation, and expression levels of NFAT3 and 4, transcription factors involved in maladaptive hypertrophy, increased by 2-fold. MAO-A inhibition with clorgyline completely prevented or significantly reduced these changes, suggesting that persistent MAO-A activation might be involved in triggering the pro-hypertrophic response via activation of pathways promoting maladaptive hypertrophy. Since NFAT activation occurs through calcineurin-dependent dephosphorylation, these data also suggest that MAO-A might contribute to hypertrophy development through the classical calcineurin/NFAT pathway.

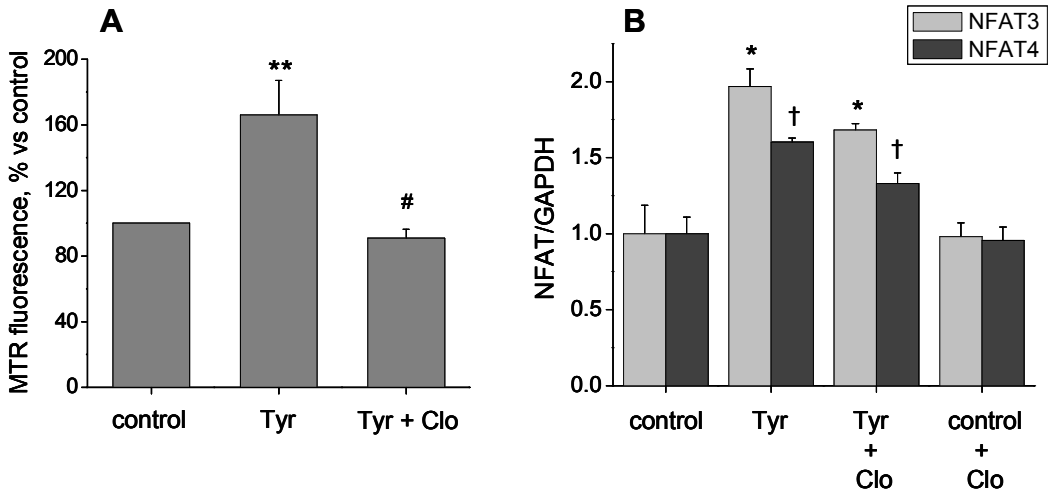

Figure 25. Effect of MAO-A activity on pro-hypertrophic signaling *in vitro*. Neonatal rat cardiomyocytes were incubated with 10 μM tyramine (Tyr) for 24 hours at 37°C. ROS production was determined by fluorescence microscopy, incubating cells with 100 nM MTR for 15 minutes at 37°C (panel A). RNA was extracted and reverse transcribed as described in Materials and Methods. Gene expression level of NFAT3 and NFAT4 (panel B) were determined by real time PCR using primers specific for those transcripts. GAPDH gene expression was used as internal control. Cells were pretreated with 1 μM clorgyline (Clo) for 1 hour prior to the addition of tyramine and clorgyline was present in the culture medium for the whole duration of the experiment.*$^{*}p<0.01$ vs control,$^{**}p<0.01$ vs control, $^{\dagger}p<0.05$ vs tyr, $^{\#}p<0.01$ vs tyr.*

5.2.2 Effects of MAO-A inhibition on the development of hypertrophy and congestive heart failure *in vivo*

We next tried to translate these *in vitro* findings into a more complex, *in vivo* setting. To this aim, we used *in vivo* model of hypertrophy and heart failure induced by pressure overload. Transverse aortic constriction (TAC) in the mouse is a commonly used surgical model of cardiac hypertrophy and subsequent failure. The aortic arch is isolated and a ligature is placed around the transverse aorta against a needle, to ensure consistent occlusion. This procedure results in 65-70% constriction after the removal of the needle and consequently, increased afterload. Cardiac adaptation to loading stress involves a complex process of chamber remodeling and myocyte molecular modifications. A fundamental response to increased biomechanical stress is cardiomyocyte hypertrophy, which manifests as an increase in myocyte size and enhanced protein synthesis. Although this response may provide important salutary compensation to the stress, prolonged hypertrophy is more often maladaptive increasing the risk of sudden death, morbidity and mortality from heart failure. Indeed, in our model compensated and concentric left ventricular hypertrophy occurs at 1 week, moderate chamber remodeling at 3 weeks and eccentric hypertrophy, characterized by chamber dilation and left ventricle dysfunction at 6 or 9 weeks of TAC.

Initially, we sought to characterize LV function and morphology during the time-course of the hypertrophy development and progression towards heart failure. This was done non-invasively, by serial m-mode echocardiography performed in conscious state. Figure 26 shows representative echocardiograms after 3 and 6 weeks of TAC, while morphologic and functional data is summarized in Table 2.

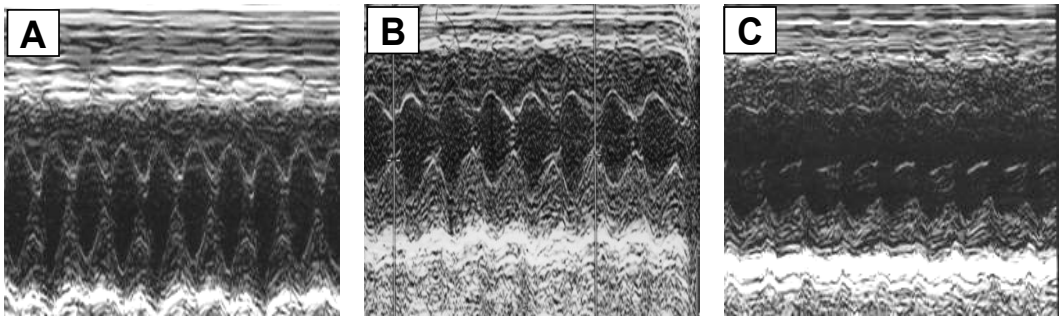

Figure 26. M-mode echocardiograms obtained in mice subjected to pressure overload. Echocardiography was performed in sham operated mice (A) and mice subjected to TAC fro 3 (B) and 6 weeks (C).

An increase in wall thickness, determined measuring septum and posterior wall diameter, was evident 3 weeks after TAC, compensating for the increase in pressure load. End-diastolic and end-systolic dimensions were unchanged or slightly increased as compared to sham mice, respectively. Both fractional shortening and ejection fraction were decreased, although the overall LV function remained compensated. All these changes became more pronounced 6 weeks after TAC. Both end-systolic and end-diastolic dimensions were increased, while septum and posterior wall thickness decreased compared to 3 weeks, indicating the occurrence of chamber dilation and eccentric hypertrophy. This was associated with depressed LV function as well. Fractional shortening and ejection fraction were further decreased and calculated LV mass showed a progressive increase form 3 to 6 weeks.

	Sham	T3w	T6w
BW (g)	27.2 ± 1.3	25.4 ± 0.6	26.6 ± 0.7
Heart rate (bpm)	738 ± 11.2	670 ± 11 *	627.5 ± 23.8 *
IVS (mm)	0.8 ± 0.02	1.3 ± 0.04 *	1.2 ± 0.04 *
LVEDD (mm)	3.2 ± 0.02	2.9 ± 0.2	4.0 ± 0.2 *†
LVESD (mm)	1.2 ± 0.02	1.7 ± 0.2	2.9 ± 0.4 *†
LVPW (mm)	0.8 ± 0.02	1.3 ± 0.04 *	1.1 ± 0.05 *
FS (%)	63.5 ± 0.9	43.9 ± 3.2 *	30.6 ± 5.3 *
EF (%)	94.7 ± 0.4	81 ± 7.9 *	62.4 ± 7.9 *†
LV mass (mg)	75.7 ± 3.2	175.2 ± 11.3 *	248.7 ± 18.5 *†
LV mass/BW (mg/g)	2.8 ± 0.1	6.9 ± 0.4 *	9.3 ± 0.5 *†

Table 2. Echocardiographic data obtained in sham operated mice and mice subjected to TAC for 3 and 6 weeks. Echocardiography was performed in conscious mice and parameters describing cardiac function were calculated as described in Materials and Methods. **p<0.005 vs sham,†p<0.005 vs T3w.*

After the characterization of the morphological and functional changes occurring in pressure overloaded hearts at these time-points, we investigated whether there were changes in MAO-A expression. MAO-A gene expression was determined at 3, 6 and 9 weeks after TAC and compared to the expression levels in sham operated animal. As shown in Figure 27, MAO-A expression dramatically increased after 6 and 9 weeks of TAC, reaching a 3.5-fold higher expression level when compared to sham operated mice. As shown previously, those two stages are associated with chamber dilation, in addition to reduced basal and β-stimulated contractility and depressed overall LV function.

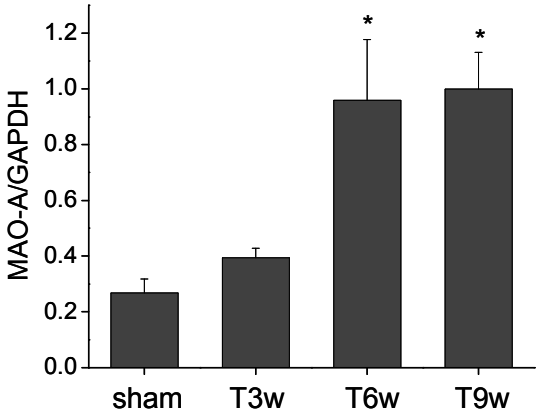

Figure 27. Changes in MAO-A gene expression in mice subjected to pressure overload. Mice were subjected to TAC for 3, 6 or 9 weeks (T3w, T6w, T9w, n=6 in each group). RNA was extracted and reverse transcribed as described in Materials and Methods. Gene expression level of MAO-A was determined by real time RT-PCR using primers specific for this transcript. GAPDH gene expression was used as internal control. **p<0.01 vs sham*.

Considering that increase in MAO-A expression was correlated with the occurrence of chamber dilation and functional decompensation, we decided to investigate whether in vivo MAO-A inhibition could contribute to maintain structural and functional order of the myocardium following TAC. To this aim, mice were subjected to TAC and randomized into saline (control) and clorgyline treated groups. As shown in Table 3, after 3 weeks of TAC wall thickness was increased in both, saline- and clorgyline-treated mice when compared to sham operated animals, likely reflecting a compensation for the increase in pressure. However, LV function was significantly better in clorgyline treated group: both fractional shortening and ejection fraction were comparable to values reported for sham mice.

	Sham	T3w	T3w + clorgyline
BW (g)	27.2 ± 1.3	25.4 ± 0.6	25.6 ± 0.6
Heart rate (bpm)	738 ± 11.2	670 ± 11 *	702 ± 12
IVS (mm)	0.8 ± 0.02	1.3 ± 0.04 *	1.3 ± 0.02 *
LVEDD (mm)	3.2 ± 0.02	2.9 ± 0.2	2.9 ± 0.06
LVESD (mm)	1.2 ± 0.02	1.7 ± 0.2	1.2 ± 0.06
LVPW (mm)	0.8 ± 0.02	1.3 ± 0.04 **	1.2 ± 0.03 **
FS (%)	63.5 ± 0.9	43.9 ± 3.2 **	56.8 ± 1.9 ‡
EF (%)	94.7 ± 0.4	81 ± 7.9 *	91.6 ± 0.4 ‡
LV mass (mg)	75.7 ± 3.2	175.2 ± 11.3 **	163.5 ± 6.7 **
LV mass/BW (mg/g)	2.8 ± 0.1	6.9 ± 0.4 **	6.4 ± 0.3 **

Table 3. Echocardiographic data obtained in sham operated mice, mice subjected to TAC for 3 weeks and mice subjected to TAC and treated with clorgyline. Echocardiography was performed in conscious mice and parameters describing cardiac function were calculated as described in Materials and Methods. **p<0.005 vs sham, **p<0.001 vs sham, ‡p<0.005 vs T3w.*

However, effects of MAO-A inhibition on the progression of heart failure became more pronounced after 6 weeks of TAC, a time-point associated with the major increase in MAO-A gene expression in control mice. Remarkably, clorgyline treated mice showed reduced cardiac hypertrophy extent and left ventricle (LV) dimensions, as shown in Figure 28.

	Sham	T6w	T6w + CLO
BW (g)	27.2 ± 1.3	26.6 ± 0.7	27.1 ± 0.4
Heart rate (bpm)	738 ± 11.2	627.5 ± 23.8 *	670 ± 13.7
IVS (mm)	0.8 ± 0.02	1.2 ± 0.04	1.4 ± 0.03 **
LVEDD (mm)	3.2 ± 0.02	4.0 ± 0.2	3.0 ± 0.08 ‡
LVESD (mm)	1.2 ± 0.02	2.9 ± 0.4 *	1.2 ± 0.04 ‡
LVPW (mm)	0.8 ± 0.02	1.1 ± 0.05 **	1.3 ± 0.03 **‡
LV mass (mg)	75.7 ± 3.2	248.7 ± 18.5 **	195.1 ± 11.5 **‡
LV mass/BW (mg/g)	2.8 ± 0.1	9.3 ± 0.5 **	7.2 ± 0.4 **‡

Table 4. Echocardiographic data obtained in sham operated mice, mice subjected to TAC for 6 weeks and mice subjected to TAC and treated with clorgyline. Echocardiography was performed in conscious mice and parameters describing cardiac function were calculated as described in Materials and Methods. **p<0.005 vs sham, **p<0.001 vs sham, ‡p<0.005 vs T6w.*

Calculated LV mass was markedly reduced in CLO-group (Table 4), and end-diastolic and end-systolic dimensions decreased from 4±0.2 and 2.9±0.4 mm to 3.1±0.1 and 1.4±0.2 mm, respectively (both $p<0.005$), paralleling the values observed in saline-treated mice. Furthermore, cardiac function was preserved in clorgyline treated group. Indeed, fractional shortening and ejection fraction went from 30±5.4 to 61±0.8% and from 60.2±8.2 to 93.6±0.4%, respectively (both $p<0.005$).

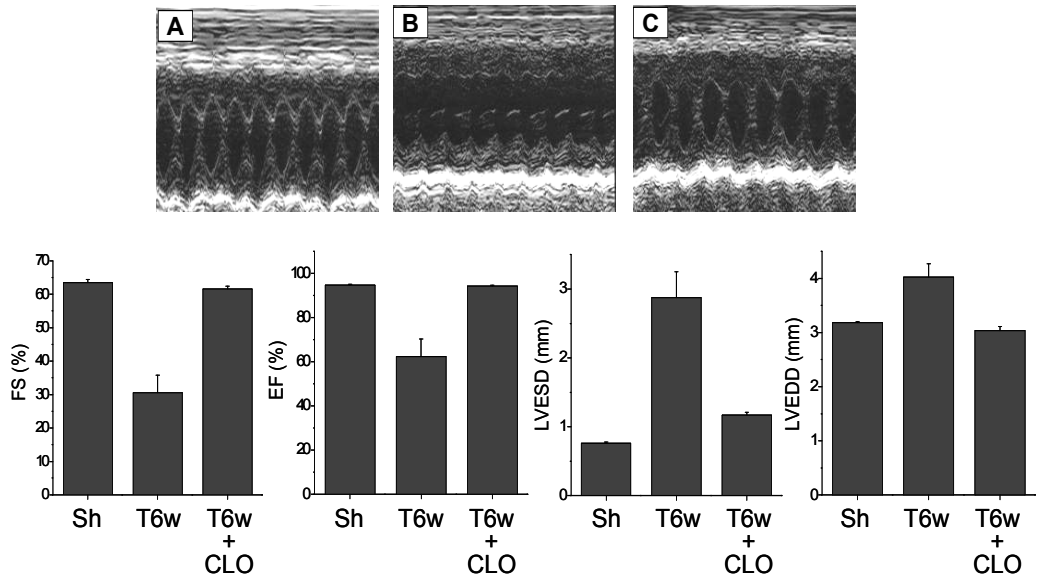

Figure 28. Effect of in vivo MAO-A inhibition on cardiac function after 6 weeks of TAC. Mice were subjected to TAC and randomized into saline- and clorgyline-treated group (1 mg/kg/day, i.p., n=6 in each group). Echocardiography was performed in conscious mice. Upper panel shows M-mode echocardiograms obtained from sham operated mice (A), mice subjected to TAC for 6 weeks (B) and mice subjected to TAC for 6 weeks and treated with clorgyline (C). Lower panel shows fractional shortening (FS), ejection fraction (EF) and end-systolic and end-diastolic diameters (LVESD and LVEDD respectively) obtained by echocardiography. **p<0.005 vs sham, †p<0.05 vs T6w*.

Myocardial hypertrophy is also accompanied by fetal gene reprogramming, reflected as the increase in ANP and BNP expression. In our model, reduced hypertrophy following clorgyline treatment was paralleled by lower fetal gene expression, as ANP rise in control TAC mice was reduced by 2-fold in clorgyline treated hearts (Fig. 29).

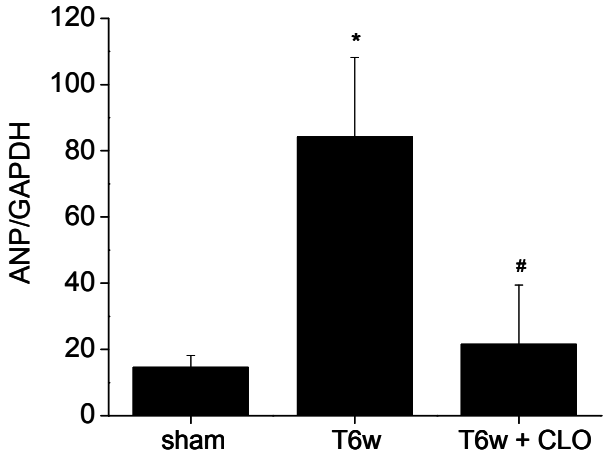

Figure 29. Effect of chronic clorgyline treatment on fetal gene re-programming in pressure overloaded mice hearts. Mice were subjected to TAC for 6 weeks (T6w) and randomized for clorgyline treatment (T6w+CLO, 1 mg/kg/day, i.p., n=6 in each group). RNA was extracted and reverse transcribed as described in Materials and Methods. Expression level of ANP was determined by real time RT-PCR using primers specific for this transcript. GAPDH gene expression was used as internal control. **p<0.05 vs sham, #p<0.05 vs T6w*.

The major positive impact of MAO-A inhibition on myocardial overall structure and function was coupled to protective effects observed at subcellular level. As mentioned before, increase in oxidative stress is often related to congestive heart failure. Therefore, we investigated whether ROS levels were increased in TAC mice and whether MAO-A inhibition was sufficient to reduce the oxidative stress *in vivo*, thereby contributing to the maintenance of cardiac function. Figure 30 shows increased oxidative stress in saline treated mice subjected to TAC for 6 weeks, as determined by DHE staining. This change was significantly reduced in clorgyline treated hearts, suggesting that MAO-A is indeed a major source of ROS that contribute to the progression of compensated hypertrophy to heart failure.

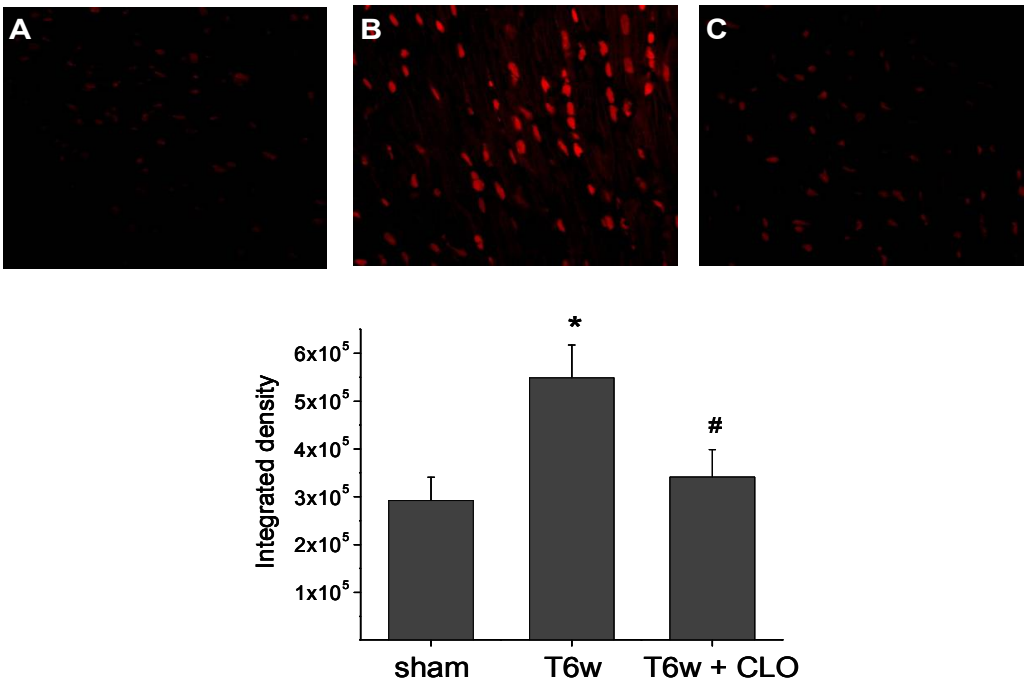

Figure 30. Effect of chronic clorgyline treatment on oxidative stress in pressure overloaded mouse hearts. Mice were subjected to TAC for 6 weeks (B) and randomized for clorgyline treatment (C, 1 mg/kg/day, i.p., n=6 in each group). LV tissue was cryosectioned, stained with DHE and visualized by fluorescence microscopy (upper panel). Area and fluorescence intensity was quantified using ImageJ software (lower panel). *$p<0.05$ vs sham, $^{\#}p<0.05$ vs T6w.

Moreover, Western blot showed decreased levels of activated Akt following clorgyline treatment, indicating blunted pro-hypertrophic signaling (Fig. 31). Although Akt activation and signaling is often associated with physiological hypertrophy, it can also be regulated by calcineurin, leading, in that case, to maladaptive hypertrophy.

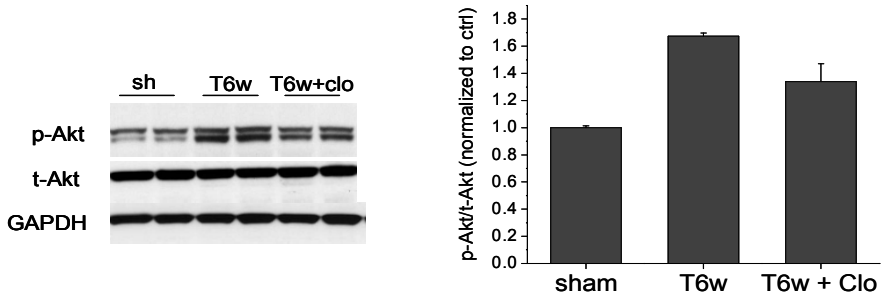

Figure 31. Effect of chronic clorgyline treatment on Akt activation in pressure overloaded mice hearts. Mice were subjected to TAC for 6 weeks (T6w) and randomized for clorgyline treatment (T6w+Clo, 1 mg/kg/day, i.p., n=6 in each group). LV tissue was homogenized and proteins analyzed by Western Blot as described in Materials and Methods. Phosphorylated Akt, total Akt and GAPDH were detected using specific antibodies. Band intensities were quantified by densitometry using ImageJ software.

As mentioned before, heart failure and impaired ventricular function are associated with a progressive thinning of myocardial wall and chamber dilation due to the loss of viable cardiomyocytes. Figure 32 shows that, after 6 weeks of TAC, there was an increase in caspase-3 activation, suggesting the activation of the pro-apoptotic cascade. This was significantly reduced in TAC hearts treated with clorgyline. Caspase-3 is activated by caspase-9, following the opening of PTP and release of cytochrome c.

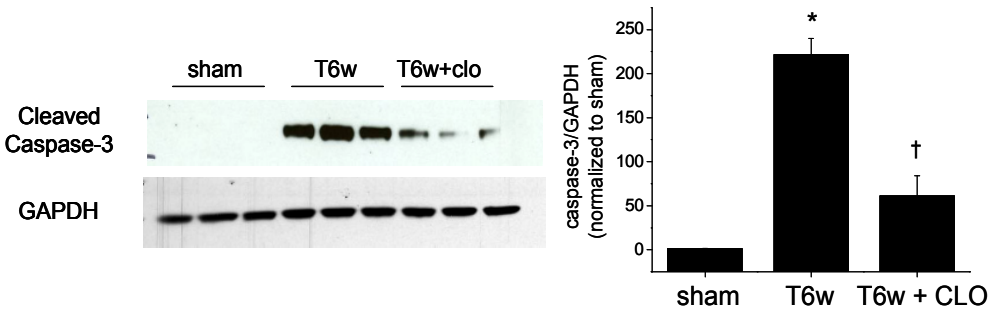

Figure 32. Effect of chronic clorgyline treatment on caspase 3 activation in pressure overloaded mice hearts. Mice were subjected to TAC for 6 weeks (T6w) and randomized for clorgyline treatment (T6w+CLO, 1 mg/kg/day, i.p., n=6 in each group). LV tissue was homogenized and proteins analyzed by Western Blot as described in Materials and Methods. Cleaved caspase 3 and GAPDH were detected using specific antibodies. Band intensities were quantified by densitometry using ImageJ software. *$*p<0.01$ vs sham, $^{\dagger}p<0.01$ vs T6w.*

Therefore, it is tempting to speculate that mitochondria might represent a direct target for MAO-generated H_2O_2, contributing to ROS-induced ROS release and leading to permeability transition pore opening, release of cytochrome c that in turn favors pro-apoptotic signaling, i.e. caspase-3 and -9 activation. Although further studies are needed to confirm this hypothesis, our data provide strong evidence that mycocyte death occurs through a mitochondrial pathway.

6 CONCLUSIONS

The results achieved in this study provide novel evidence regarding the sources of ROS at mitochondrial level in relation to the development of hypertrophy and congestive heart failure. It is widely accepted that mitochondrial respiratory chain can become a powerful generator of ROS, especially under conditions of increased stress. It is also becoming increasingly clear that other mitochondrial enzymes play an important role in this process. Here we have demonstrated that MAO-A is a major source of ROS in the mitochondria and that its inhibition can prevent oxidative stress in the cardiomyocytes. Indeed, exposure of the cells to pro-apoptotic agents, such as H_2O_2 and arachidonic acid induced an early increase in oxidative stress followed by cell death. This increase in ROS production requires the intervention of MAO-A, as its pharmacological inhibition was able to reduce or completely prevent the oxidative stress in cardiac myocytes. Remarkably, identical results were obtained when MAO-A protein expression was reduced by 90% by means of siRNA, confirming the specificity of the inhibitors used and the importance of the A isoform of the enzyme, as compared to the B isoform, which does not seem to play a relevant role in the oxidative stress, at least at the cardiomyocyte level. The role of MAO-A could be interpreted as a trigger necessary to amplify the initial oxidative stimuli and therefore contribute to the instauration of oxidative stress and cellular dysfunction.

Oxidative stress underlies many pathologies. At the cardiac level, the involvement of oxidative stress has been demonstrated to contribute to ischemia/reperfusion injury and hypertrophy development, especially in the latter phases when extensive remodeling of the left ventricle occurs, progressively leading to congestive heart failure. The results obtained in this study support this hypothesis and reveal that MAO-A is involved in these processes.

In vitro studies in neonatal rat cardiomyocytes, demonstrate that pro-hypertrophic stimuli can induce MAO-A gene expression and that its activity contributes to the development of maladaptive hypertrophy. The latter observation is supported by the fact that persistent stimulation of MAO-A activity can trigger the activation of NFAT3 and NFAT4, two transcription factors involved in maladaptive hypertrophy. These changes are likely attributable to increased ROS

formation due to MAO-A activity, as clorgyline was able to prevent or reduce these effects. MAO-A inhibition has also been shown to reduce norepinephrine induced hypertrophy. While norepinephrine has been previously associated with increased ROS formation through activation of α,β-adrenergic receptors-mediated signal transduction pathways, the evidence provided in the present work suggests that this hormone, whose levels are increased in heart failure, might also be transported into the myocytes through transporters present at the membrane level and catabolyzed by MAO therefore contributing to increased ROS signaling.

More importantly, the involvement of MAO-A was also investigated in *in vivo* hypertrophy and congestive heart failure. Mice subjected to transverse aortic constriction resulting in pressure overload, display 3.5 fold increase in MAO-A gene expression at a time-point associated with chamber dilation, left ventricle dysfunction and overall pump failure. *In vivo* pharmacological inhibition of MAO-A in these mice resulted in decreased levels of hypertrophy and preserved LV function. Clorgyline treatment completely prevented chamber dilation and functional decompensation, as clorgyline treated mice showed morphological and functional parameters comparable to those observed in sham operated mice, in which no pressure overload was induced. The observation that oxidative stress was reduced in clorgyline treated mice suggests that MAO A-derived ROS contribute to a great extent to cardiac remodeling.

Finally, in vivo MAO-A inhibition also reduced activation of caspase-3, involved in pro-apoptotic signaling. This finding supports the hypothesis that the loss of viable cardiomyocytes is responsible for functional decompensation and occurrence of heart failure. Moreover, since caspase activation lies downstream of mitochondrial dysfunction in the pro-apoptotic cascade, it is likely that mitochondria represent a target for MAO A-derived ROS resulting in permeability transition pore opening, release of cytochrome c and other pro-apoptotic factors leading to cell death.

In conclusion, MAO-A is an important source of ROS in cardiac myocytes. Its inhibition is able to preserve structural and functional myocardial order in mice subjected to pressure overload and prevent the transition of compensated hypertrophy to congestive heart failure. Thus, MAO-A inhibition may represent a new therapeutic tool for the treatment of cardiac disease.

7 REFERENCE LIST

(1) Chen ZY, Powell JF, Hsu YP, Breakefield XO, Craig IW. Organization of the human monoamine oxidase genes and long-range physical mapping around them. *Genomics* 1992 September;14(1):75-82.

(2) Grimsby J, Chen K, Wang LJ, Lan NC, Shih JC. Human monoamine oxidase A and B genes exhibit identical exon-intron organization. *Proc Natl Acad Sci U S A* 1991 May 1;88(9):3637-41.

(3) Bach AW, Lan NC, Johnson DL et al. cDNA cloning of human liver monoamine oxidase A and B: molecular basis of differences in enzymatic properties. *Proc Natl Acad Sci U S A* 1988 July;85(13):4934-8.

(4) Edmondson DE, Mattevi A, Binda C, Li M, Hubalek F. Structure and mechanism of monoamine oxidase. *Curr Med Chem* 2004 August;11(15):1983-93.

(5) Chen ZY, Hotamisligil GS, Huang JK et al. Structure of the human gene for monoamine oxidase type A. *Nucleic Acids Res* 1991 August 25;19(16):4537-41.

(6) Edmondson DE, Binda C, Mattevi A. The FAD binding sites of human monoamine oxidases A and B. *Neurotoxicology* 2004 January;25(1-2):63-72.

(7) Abell CW, Kwan SW. Molecular characterization of monoamine oxidases A and B. *Prog Nucleic Acid Res Mol Biol* 2001;65:129-56.

(8) Binda C, Newton-Vinson P, Hubalek F, Edmondson DE, Mattevi A. Structure of human monoamine oxidase B, a drug target for the treatment of neurological disorders. *Nat Struct Biol* 2002 January;9(1):22-6.

(9) De CL, Li M, Binda C, Lustig A, Edmondson DE, Mattevi A. Three-dimensional structure of human monoamine oxidase A (MAO A): relation to the structures of rat MAO A and human MAO B. *Proc Natl Acad Sci U S A* 2005 September 6;102(36):12684-9.

(10) Binda C, Li M, Hubalek F, Restelli N, Edmondson DE, Mattevi A. Insights into the mode of inhibition of human mitochondrial monoamine oxidase B from high-resolution crystal structures. *Proc Natl Acad Sci U S A* 2003 August 19;100(17):9750-5.

(11) Kearney EB, Salach JI, Walker WH et al. The covalently-bound flavin of hepatic monoamine oxidase. 1. Isolation and sequence of a flavin peptide and evidence for binding at the 8alpha position. *Eur J Biochem* 1971 December;24(2):321-7.

(12) Youdim MB, Edmondson D, Tipton KF. The therapeutic potential of monoamine oxidase inhibitors. *Nat Rev Neurosci* 2006 April;7(4):295-309.

(13) Tipton KF, Boyce S, O'Sullivan J, Davey GP, Healy J. Monoamine oxidases: certainties and uncertainties. *Curr Med Chem* 2004 August;11(15):1965-82.

(14) Cases O, Seif I, Grimsby J et al. Aggressive behavior and altered amounts of brain serotonin and norepinephrine in mice lacking MAOA. *Science* 1995 June 23;268(5218):1763-6.

(15) Lenders JW, Eisenhofer G, Abeling NG et al. Specific genetic deficiencies of the A and B isoenzymes of monoamine oxidase are characterized by distinct neurochemical and clinical phenotypes. *J Clin Invest* 1996 February 15;97(4):1010-9.

(16) Brunner HG, Nelen M, Breakefield XO, Ropers HH, van Oost BA. Abnormal behavior associated with a point mutation in the structural gene for monoamine oxidase A. *Science* 1993 October 22;262(5133):578-80.

(17) Shih JC. Cloning, after cloning, knock-out mice, and physiological functions of MAO A and B. *Neurotoxicology* 2004 January;25(1-2):21-30.

(18) Rebsam A, Seif I, Gaspar P. Dissociating barrel development and lesion-induced plasticity in the mouse somatosensory cortex. *J Neurosci* 2005 January 19;25(3):706-10.

(19) Berry MD, Juorio AV, Paterson IA. The functional role of monoamine oxidases A and B in the mammalian central nervous system. *Prog Neurobiol* 1994 February;42(3):375-91.

(20) Kitahama K, Maeda T, Denney RM, Jouvet M. Monoamine oxidase: distribution in the cat brain studied by enzyme- and immunohistochemistry: recent progress. *Prog Neurobiol* 1994 January;42(1):53-78.

(21) Luque JM, Biou V, Nicholls JG. Three-dimensional visualization of the distribution, growth, and regeneration of monoaminergic neurons in whole mounts of immature mammalian CNS. *J Comp Neurol* 1998 January 19;390(3):427-38.

(22) Arai R, Kimura H, Nagatsu I, Maeda T. Preferential localization of monoamine oxidase type A activity in neurons of the locus coeruleus and type B activity in neurons of the dorsal raphe nucleus of the rat: a detailed enzyme histochemical study. *Brain Res* 1997 January 16;745(1-2):352-6.

(23) Levitt P, Pintar JE, Breakefield XO. Immunocytochemical demonstration of monoamine oxidase B in brain astrocytes and

serotonergic neurons. *Proc Natl Acad Sci U S A* 1982 October;79(20):6385-9.

(24) Westlund KN, Denney RM, Kochersperger LM, Rose RM, Abell CW. Distinct monoamine oxidase A and B populations in primate brain. *Science* 1985 October 11;230(4722):181-3.

(25) Westlund KN, Denney RM, Rose RM, Abell CW. Localization of distinct monoamine oxidase A and monoamine oxidase B cell populations in human brainstem. *Neuroscience* 1988 May;25(2):439-56.

(26) Fowler JS, Logan J, Wang GJ et al. Monoamine oxidase A imaging in peripheral organs in healthy human subjects. *Synapse* 2003 September 1;49(3):178-87.

(27) Sivasubramaniam SD, Finch CC, Rodriguez MJ, Mahy N, Billett EE. A comparative study of the expression of monoamine oxidase-A and -B mRNA and protein in non-CNS human tissues. *Cell Tissue Res* 2003 September;313(3):291-300.

(28) Saura J, Kettler R, Da PM, Richards JG. Quantitative enzyme radioautography with 3H-Ro 41-1049 and 3H-Ro 19-6327 in vitro: localization and abundance of MAO-A and MAO-B in rat CNS, peripheral organs, and human brain. *J Neurosci* 1992 May;12(5):1977-99.

(29) Shih JC, Chen K. Regulation of MAO-A and MAO-B gene expression. *Curr Med Chem* 2004 August;11(15):1995-2005.

(30) Edelstein SB, Breakefield XO. Monoamine oxidases A and B are differentially regulated by glucocorticoids and "aging" in human skin fibroblasts. *Cell Mol Neurobiol* 1986 June;6(2):121-50.

(31) Youdim MB, Banerjee DK, Kelner K, Offutt L, Pollard HB. Steroid regulation of monoamine oxidase activity in the adrenal medulla. *FASEB J* 1989 April;3(6):1753-9.

(32) Zhu QS, Grimsby J, Chen K, Shih JC. Promoter organization and activity of human monoamine oxidase (MAO) A and B genes. *J Neurosci* 1992 November;12(11):4437-46.

(33) Zhu QS, Chen K, Shih JC. Bidirectional promoter of human monoamine oxidase A (MAO A) controlled by transcription factor Sp1. *J Neurosci* 1994 December;14(12):7393-403.

(34) Yang L, Omori K, Suzukawa J, Inagaki C. Calcineurin-mediated BAD Ser155 dephosphorylation in ammonia-induced apoptosis of cultured rat hippocampal neurons. *Neurosci Lett* 2004 February 26;357(1):73-5.

(35) Halliwell B. Reactive oxygen species and the central nervous system. *J Neurochem* 1992 November;59(5):1609-23.

(36) Cesura AM, Pletscher A. The new generation of monoamine oxidase inhibitors. *Prog Drug Res* 1992;38:171-297.

(37) Bianchi P, Kunduzova O, Masini E et al. Oxidative stress by monoamine oxidase mediates receptor-independent cardiomyocyte apoptosis by serotonin and postischemic myocardial injury. *Circulation* 2005 November 22;112(21):3297-305.

(38) Pchejetski D, Kunduzova O, Dayon A et al. Oxidative stress-dependent sphingosine kinase-1 inhibition mediates monoamine oxidase A-associated cardiac cell apoptosis. *Circ Res* 2007 January 5;100(1):41-9.

(39) Bianchi P, Pimentel DR, Murphy MP, Colucci WS, Parini A. A new hypertrophic mechanism of serotonin in cardiac myocytes: receptor-independent ROS generation. *FASEB J* 2005 April;19(6):641-3.

(40) Coatrieux C, Sanson M, Negre-Salvayre A et al. MAO-A-induced mitogenic signaling is mediated by reactive oxygen species, MMP-2, and the sphingolipid pathway. *Free Radic Biol Med* 2007 July 1;43(1):80-9.

(41) Maurel A, Hernandez C, Kunduzova O et al. Age-dependent increase in hydrogen peroxide production by cardiac monoamine oxidase A in rats. *Am J Physiol Heart Circ Physiol* 2003 April;284(4):H1460-H1467.

(42) Riederer P, Lachenmayer L, Laux G. Clinical applications of MAO-inhibitors. *Curr Med Chem* 2004 August;11(15):2033-43.

(43) Riederer P, Lachenmayer L, Laux G. Clinical applications of MAO-inhibitors. *Curr Med Chem* 2004 August;11(15):2033-43.

(44) Dostert PL, Strolin BM, Tipton KF. Interactions of monoamine oxidase with substrates and inhibitors. *Med Res Rev* 1989 January;9(1):45-89.

(45) Pletscher A. The discovery of antidepressants: a winding path. *Experientia* 1991 January 15;47(1):4-8.

(46) Tetrud JW, Koller WC. A novel formulation of selegiline for the treatment of Parkinson's disease. *Neurology* 2004 October 12;63(7 Suppl 2):S2-S6.

(47) Marin DB, Bierer LM, Lawlor BA et al. L-deprenyl and physostigmine for the treatment of Alzheimer's disease. *Psychiatry Res* 1995 October 16;58(3):181-9.

(48) Qin F, Shite J, Mao W, Liang CS. Selegiline attenuates cardiac oxidative stress and apoptosis in heart failure: association with improvement of cardiac function. *Eur J Pharmacol* 2003 February 14;461(2-3):149-58.

(49) Simon L, Szilagyi G, Bori Z, Orbay P, Nagy Z. (-)-D-Deprenyl attenuates apoptosis in experimental brain ischaemia. *Eur J Pharmacol* 2001 November 2;430(2-3):235-41.

(50) Vondriska TM, Klein JB, Ping P. Use of functional proteomics to investigate PKC epsilon-mediated cardioprotection: the signaling module hypothesis. *Am J Physiol Heart Circ Physiol* 2001 April;280(4):H1434-H1441.

(51) Weinreb O, Bar-Am O, Amit T, Chillag-Talmor O, Youdim MB. Neuroprotection via pro-survival protein kinase C isoforms associated with Bcl-2 family members. *FASEB J* 2004 September;18(12):1471-3.

(52) Stadtman ER, Levine RL. Protein oxidation. *Ann N Y Acad Sci* 2000;899:191-208.

(53) Davies KJ. Oxidative stress: the paradox of aerobic life. *Biochem Soc Symp* 1995;61:1-31.

(54) Ide T, Tsutsui H, Kinugawa S et al. Mitochondrial electron transport complex I is a potential source of oxygen free radicals in the failing myocardium. *Circ Res* 1999 August 20;85(4):357-63.

(55) Finkel T, Holbrook NJ. Oxidants, oxidative stress and the biology of ageing. *Nature* 2000 November 9;408(6809):239-47.

(56) Droge W. Free radicals in the physiological control of cell function. *Physiol Rev* 2002 January;82(1):47-95.

(57) Davies MJ. Singlet oxygen-mediated damage to proteins and its consequences. *Biochem Biophys Res Commun* 2003 June 6;305(3):761-70.

(58) Liochev SI, Fridovich I. The relative importance of HO* and. *Free Radic Biol Med* 1999 March;26(5-6):777-8.

(59) Stadtman ER, Berlett BS. Fenton chemistry. Amino acid oxidation. *J Biol Chem* 1991 September 15;266(26):17201-11.

(60) Marnett LJ. Oxyradicals and DNA damage. *Carcinogenesis* 2000 March;21(3):361-70.

(61) Nordberg J, Arner ES. Reactive oxygen species, antioxidants, and the mammalian thioredoxin system. *Free Radic Biol Med* 2001 December 1;31(11):1287-312.

(62) Cadenas E, Davies KJ. Mitochondrial free radical generation, oxidative stress, and aging. *Free Radic Biol Med* 2000 August;29(3-4):222-30.

(63) Pacifici RE, Davies KJ. Protein, lipid and DNA repair systems in oxidative stress: the free-radical theory of aging revisited. *Gerontology* 1991;37(1-3):166-80.

(64) Sitte N, Huber M, Grune T et al. Proteasome inhibition by lipofuscin/ceroid during postmitotic aging of fibroblasts. *FASEB J* 2000 August;14(11):1490-8.

(65) Halliwell B. The role of oxygen radicals in human disease, with particular reference to the vascular system. *Haemostasis* 1993 March;23 Suppl 1:118-26.

(66) Okado-Matsumoto A, Fridovich I. Subcellular distribution of superoxide dismutases (SOD) in rat liver: Cu,Zn-SOD in mitochondria. *J Biol Chem* 2001 October 19;276(42):38388-93.

(67) Weisiger RA, Fridovich I. Superoxide dismutase. Organelle specificity. *J Biol Chem* 1973 May 25;248(10):3582-92.

(68) Ursini F, Maiorino M, Brigelius-Flohe R et al. Diversity of glutathione peroxidases. *Methods Enzymol* 1995;252:38-53.

(69) Urso ML, Clarkson PM. Oxidative stress, exercise, and antioxidant supplementation. *Toxicology* 2003 July 15;189(1-2):41-54.

(70) Traber MG, Atkinson J. Vitamin E, antioxidant and nothing more. *Free Radic Biol Med* 2007 July 1;43(1):4-15.

(71) Meister A. Glutathione-ascorbic acid antioxidant system in animals. *J Biol Chem* 1994 April 1;269(13):9397-400.

(72) MacLean PD, Drake EC, Ross L, Barclay C. Bilirubin as an antioxidant in micelles and lipid bilayers: its contribution to the total antioxidant capacity of human blood plasma. *Free Radic Biol Med* 2007 August 15;43(4):600-9.

(73) Waring WS. Uric acid: an important antioxidant in acute ischaemic stroke. *QJM* 2002 October;95(10):691-3.

(74) Votyakova TV, Reynolds IJ. DeltaPsi(m)-Dependent and -independent production of reactive oxygen species by rat brain mitochondria. *J Neurochem* 2001 October;79(2):266-77.

(75) Boveris A, Chance B. The mitochondrial generation of hydrogen peroxide. General properties and effect of hyperbaric oxygen. *Biochem J* 1973 July;134(3):707-16.

(76) Giorgio M, Migliaccio E, Orsini F et al. Electron transfer between cytochrome c and p66Shc generates reactive oxygen species that trigger mitochondrial apoptosis. *Cell* 2005 July 29;122(2):221-33.

(77) Trinei M, Giorgio M, Cicalese A et al. A p53-p66Shc signalling pathway controls intracellular redox status, levels of oxidation-damaged DNA and oxidative stress-induced apoptosis. *Oncogene* 2002 May 30;21(24):3872-8.

(78) Orsini F, Migliaccio E, Moroni M et al. The life span determinant p66Shc localizes to mitochondria where it associates with mitochondrial heat shock protein 70 and regulates trans-membrane potential. *J Biol Chem* 2004 June 11;279(24):25689-95.

(79) Zaccagnini G, Martelli F, Fasanaro P et al. p66ShcA modulates tissue response to hindlimb ischemia. *Circulation* 2004 June 15;109(23):2917-23.

(80) Taylor SW, Fahy E, Murray J, Capaldi RA, Ghosh SS. Oxidative post-translational modification of tryptophan residues in cardiac mitochondrial proteins. *J Biol Chem* 2003 May 30;278(22):19587-90.

(81) Murray J, Taylor SW, Zhang B, Ghosh SS, Capaldi RA. Oxidative damage to mitochondrial complex I due to peroxynitrite: identification of reactive tyrosines by mass spectrometry. *J Biol Chem* 2003 September 26;278(39):37223-30.

(82) Turrens JF. Mitochondrial formation of reactive oxygen species. *J Physiol* 2003 October 15;552(Pt 2):335-44.

(83) Barja G. Mitochondrial free radical production and aging in mammals and birds. *Ann N Y Acad Sci* 1998 November 20;854:224-38.

(84) Barrientos A, Moraes CT. Titrating the effects of mitochondrial complex I impairment in the cell physiology. *J Biol Chem* 1999 June 4;274(23):16188-97.

(85) Petrosillo G, Ruggiero FM, Pistolese M, Paradies G. Ca2+-induced reactive oxygen species production promotes cytochrome c release from rat liver mitochondria via mitochondrial permeability transition (MPT)-dependent and MPT-independent mechanisms: role of cardiolipin. *J Biol Chem* 2004 December 17;279(51):53103-8.

(86) Di LF, Bernardi P. Mitochondrial function and myocardial aging. A critical analysis of the role of permeability transition. *Cardiovasc Res* 2005 May 1;66(2):222-32.

(87) Di LF, Bernardi P. Mitochondria and ischemia-reperfusion injury of the heart: fixing a hole. *Cardiovasc Res* 2006 May 1;70(2):191-9.

(88) Petronilli V, Cola C, Massari S, Colonna R, Bernardi P. Physiological effectors modify voltage sensing by the cyclosporin A-sensitive permeability transition pore of mitochondria. *J Biol Chem* 1993 October 15;268(29):21939-45.

(89) Bernardi P, Vassanelli S, Veronese P, Colonna R, Szabo I, Zoratti M. Modulation of the mitochondrial permeability transition pore. Effect of protons and divalent cations. *J Biol Chem* 1992 February 15;267(5):2934-9.

(90) Bernardi P. Modulation of the mitochondrial cyclosporin A-sensitive permeability transition pore by the proton electrochemical gradient. Evidence that the pore can be opened by membrane depolarization. *J Biol Chem* 1992 May 5;267(13):8834-9.

(91) Halestrap AP, Kerr PM, Javadov S, Woodfield KY. Elucidating the molecular mechanism of the permeability transition pore and its role in reperfusion injury of the heart. *Biochim Biophys Acta* 1998 August 10;1366(1-2):79-94.

(92) Zoratti M, Szabo I. The mitochondrial permeability transition. *Biochim Biophys Acta* 1995 July 17;1241(2):139-76.

(93) Di LF, Bernardi P. Mitochondrial function as a determinant of recovery or death in cell response to injury. *Mol Cell Biochem* 1998 July;184(1-2):379-91.

(94) Zorov DB, Filburn CR, Klotz LO, Zweier JL, Sollott SJ. Reactive oxygen species (ROS)-induced ROS release: a new phenomenon accompanying induction of the mitochondrial permeability transition in cardiac myocytes. *J Exp Med* 2000 October 2;192(7):1001-14.

(95) Brill A, Torchinsky A, Carp H, Toder V. The role of apoptosis in normal and abnormal embryonic development. *J Assist Reprod Genet* 1999 November;16(10):512-9.

(96) Steller H. Mechanisms and genes of cellular suicide. *Science* 1995 March 10;267(5203):1445-9.

(97) Lowe SW, Lin AW. Apoptosis in cancer. *Carcinogenesis* 2000 March;21(3):485-95.

(98) Haunstetter A, Izumo S. Future perspectives and potential implications of cardiac myocyte apoptosis. *Cardiovasc Res* 2000 February;45(3):795-801.

(99) Badley AD, Dockrell D, Paya CV. Apoptosis in AIDS. *Adv Pharmacol* 1997;41:271-94.

(100) Liu X, Kim CN, Yang J, Jemmerson R, Wang X. Induction of apoptotic program in cell-free extracts: requirement for dATP and cytochrome c. *Cell* 1996 July 12;86(1):147-57.

(101) Ankarcrona M, Dypbukt JM, Bonfoco E et al. Glutamate-induced neuronal death: a succession of necrosis or apoptosis depending on mitochondrial function. *Neuron* 1995 October;15(4):961-73.

(102) Qian T, Herman B, Lemasters JJ. The mitochondrial permeability transition mediates both necrotic and apoptotic death of hepatocytes exposed to Br-A23187. *Toxicol Appl Pharmacol* 1999 January 15;154(2):117-25.

(103) Jennings RB, Ganote CE. Mitochondrial structure and function in acute myocardial ischemic injury. *Circ Res* 1976 May;38(5 Suppl 1):I80-I91.

(104) Di LF, Canton M, Menabo R, Kaludercic N, Bernardi P. Mitochondria and cardioprotection. *Heart Fail Rev* 2007 December;12(3-4):249-60.

(105) Bernardi P, Krauskopf A, Basso E et al. The mitochondrial permeability transition from in vitro artifact to disease target. *FEBS J* 2006 May;273(10):2077-99.

(106) Weiss JN, Korge P, Honda HM, Ping P. Role of the mitochondrial permeability transition in myocardial disease. *Circ Res* 2003 August 22;93(4):292-301.

(107) Ide T, Tsutsui H, Hayashidani S et al. Mitochondrial DNA damage and dysfunction associated with oxidative stress in failing hearts after myocardial infarction. *Circ Res* 2001 March 16;88(5):529-35.

(108) Marin-Garcia J, Goldenthal MJ, Moe GW. Abnormal cardiac and skeletal muscle mitochondrial function in pacing-induced cardiac failure. *Cardiovasc Res* 2001 October;52(1):103-10.

(109) Quigley AF, Kapsa RM, Esmore D, Hale G, Byrne E. Mitochondrial respiratory chain activity in idiopathic dilated cardiomyopathy. *J Card Fail* 2000 March;6(1):47-55.

(110) Casademont J, Miro O. Electron transport chain defects in heart failure. *Heart Fail Rev* 2002 April;7(2):131-9.

(111) Lewandowski ED. Cardiac carbon 13 magnetic resonance spectroscopy: on the horizon or over the rainbow? *J Nucl Cardiol* 2002 July;9(4):419-28.

(112) Murray AJ, Anderson RE, Watson GC, Radda GK, Clarke K. Uncoupling proteins in human heart. *Lancet* 2004 November 13;364(9447):1786-8.

(113) Marin-Garcia J, Goldenthal MJ, Moe GW. Mitochondrial pathology in cardiac failure. *Cardiovasc Res* 2001 January;49(1):17-26.

(114) Scheubel RJ, Tostlebe M, Simm A et al. Dysfunction of mitochondrial respiratory chain complex I in human failing myocardium is not due to disturbed mitochondrial gene expression. *J Am Coll Cardiol* 2002 December 18;40(12):2174-81.

(115) Neubauer S. The failing heart--an engine out of fuel. *N Engl J Med* 2007 March 15;356(11):1140-51.

(116) Radford NB, Wan B, Richman A et al. Cardiac dysfunction in mice lacking cytochrome-c oxidase subunit VIaH. *Am J Physiol Heart Circ Physiol* 2002 February;282(2):H726-H733.

(117) Graham BH, Waymire KG, Cottrell B, Trounce IA, MacGregor GR, Wallace DC. A mouse model for mitochondrial myopathy and cardiomyopathy resulting from a deficiency in the heart/muscle isoform of the adenine nucleotide translocator. *Nat Genet* 1997 July;16(3):226-34.

(118) Arany Z, Novikov M, Chin S, Ma Y, Rosenzweig A, Spiegelman BM. Transverse aortic constriction leads to accelerated heart failure in mice lacking PPAR-gamma coactivator 1alpha. *Proc Natl Acad Sci U S A* 2006 June 27;103(26):10086-91.

(119) Watanabe K, Fujii H, Takahashi T et al. Constitutive regulation of cardiac fatty acid metabolism through peroxisome proliferator-activated receptor alpha associated with age-dependent cardiac toxicity. *J Biol Chem* 2000 July 21;275(29):22293-9.

(120) Li Y, Huang TT, Carlson EJ et al. Dilated cardiomyopathy and neonatal lethality in mutant mice lacking manganese superoxide dismutase. *Nat Genet* 1995 December;11(4):376-81.

(121) Frey N, Olson EN. Cardiac hypertrophy: the good, the bad, and the ugly. *Annu Rev Physiol* 2003;65:45-79.

(122) Kang PM, Izumo S. Apoptosis in heart: basic mechanisms and implications in cardiovascular diseases. *Trends Mol Med* 2003 April;9(4):177-82.

(123) Molkentin JD, Lu JR, Antos CL et al. A calcineurin-dependent transcriptional pathway for cardiac hypertrophy. *Cell* 1998 April 17;93(2):215-28.

(124) Wilkins BJ, De Windt LJ, Bueno OF et al. Targeted disruption of NFATc3, but not NFATc4, reveals an intrinsic defect in calcineurin-mediated cardiac hypertrophic growth. *Mol Cell Biol* 2002 November;22(21):7603-13.

(125) Molkentin JD, Dorn II GW. Cytoplasmic signaling pathways that regulate cardiac hypertrophy. *Annu Rev Physiol* 2001;63:391-426.

(126) Frey N, McKinsey TA, Olson EN. Decoding calcium signals involved in cardiac growth and function. *Nat Med* 2000 November;6(11):1221-7.

(127) Sugden PH. Signalling pathways in cardiac myocyte hypertrophy. *Ann Med* 2001 December;33(9):611-22.

(128) Dorn GW, Force T. Protein kinase cascades in the regulation of cardiac hypertrophy. *J Clin Invest* 2005 March;115(3):527-37.

(129) Cantley LC. The phosphoinositide 3-kinase pathway. *Science* 2002 May 31;296(5573):1655-7.

(130) Shioi T, Kang PM, Douglas PS et al. The conserved phosphoinositide 3-kinase pathway determines heart size in mice. *EMBO J* 2000 June 1;19(11):2537-48.

(131) Patrucco E, Notte A, Barberis L et al. PI3Kgamma modulates the cardiac response to chronic pressure overload by distinct kinase-dependent and -independent effects. *Cell* 2004 August 6;118(3):375-87.

(132) DeBosch B, Treskov I, Lupu TS et al. Akt1 is required for physiological cardiac growth. *Circulation* 2006 May 2;113(17):2097-104.

(133) Antos CL, McKinsey TA, Frey N et al. Activated glycogen synthase-3 beta suppresses cardiac hypertrophy in vivo. *Proc Natl Acad Sci U S A* 2002 January 22;99(2):907-12.

(134) Bueno OF, De Windt LJ, Tymitz KM et al. The MEK1-ERK1/2 signaling pathway promotes compensated cardiac hypertrophy in transgenic mice. *EMBO J* 2000 December 1;19(23):6341-50.

(135) Sanna B, Bueno OF, Dai YS, Wilkins BJ, Molkentin JD. Direct and indirect interactions between calcineurin-NFAT and MEK1-extracellular signal-regulated kinase 1/2 signaling pathways regulate cardiac gene expression and cellular growth. *Mol Cell Biol* 2005 February;25(3):865-78.

(136) Liao P, Georgakopoulos D, Kovacs A et al. The in vivo role of p38 MAP kinases in cardiac remodeling and restrictive cardiomyopathy. *Proc Natl Acad Sci U S A* 2001 October 9;98(21):12283-8.

(137) Petrich BG, Molkentin JD, Wang Y. Temporal activation of c-Jun N-terminal kinase in adult transgenic heart via cre-loxP-mediated DNA recombination. *FASEB J* 2003 April;17(6):749-51.

(138) Giordano FJ. Oxygen, oxidative stress, hypoxia, and heart failure. *J Clin Invest* 2005 March;115(3):500-8.

(139) Takimoto E, Kass DA. Role of oxidative stress in cardiac hypertrophy and remodeling. *Hypertension* 2007 February;49(2):241-8.

(140) Sugden PH, Clerk A. Oxidative stress and growth-regulating intracellular signaling pathways in cardiac myocytes. *Antioxid Redox Signal* 2006 November;8(11-12):2111-24.

(141) Nakamura K, Fushimi K, Kouchi H et al. Inhibitory effects of antioxidants on neonatal rat cardiac myocyte hypertrophy induced by tumor necrosis factor-alpha and angiotensin II. *Circulation* 1998 August 25;98(8):794-9.

(142) Luo JD, Xie F, Zhang WW, Ma XD, Guan JX, Chen X. Simvastatin inhibits noradrenaline-induced hypertrophy of cultured neonatal rat cardiomyocytes. *Br J Pharmacol* 2001 January;132(1):159-64.

(143) Kwon SH, Pimentel DR, Remondino A, Sawyer DB, Colucci WS. H(2)O(2) regulates cardiac myocyte phenotype via concentration-dependent activation of distinct kinase pathways. *J Mol Cell Cardiol* 2003 June;35(6):615-21.

(144) Hirotani S, Otsu K, Nishida K et al. Involvement of nuclear factor-kappaB and apoptosis signal-regulating kinase 1 in G-protein-coupled

receptor agonist-induced cardiomyocyte hypertrophy. *Circulation* 2002 January 29;105(4):509-15.

(145) Yamaguchi O, Higuchi Y, Hirotani S et al. Targeted deletion of apoptosis signal-regulating kinase 1 attenuates left ventricular remodeling. *Proc Natl Acad Sci U S A* 2003 December 23;100(26):15883-8.

(146) Siwik DA, Pagano PJ, Colucci WS. Oxidative stress regulates collagen synthesis and matrix metalloproteinase activity in cardiac fibroblasts. *Am J Physiol Cell Physiol* 2001 January;280(1):C53-C60.

(147) Siwik DA, Colucci WS. Regulation of matrix metalloproteinases by cytokines and reactive oxygen/nitrogen species in the myocardium. *Heart Fail Rev* 2004 January;9(1):43-51.

(148) Zima AV, Blatter LA. Redox regulation of cardiac calcium channels and transporters. *Cardiovasc Res* 2006 July 15;71(2):310-21.

(149) Laemmli UK. Cleavage of structural proteins during the assembly of the head of bacteriophage T4. *Nature* 1970 August 15;227(5259):680-5.

(150) Towbin H, Staehelin T, Gordon J. Electrophoretic transfer of proteins from polyacrylamide gels to nitrocellulose sheets: procedure and some applications. *Proc Natl Acad Sci U S A* 1979 September;76(9):4350-4.

(151) Claycomb WC, Lanson NA, Jr., Stallworth BS et al. HL-1 cells: a cardiac muscle cell line that contracts and retains phenotypic characteristics of the adult cardiomyocyte. *Proc Natl Acad Sci U S A* 1998 March 17;95(6):2979-84.

(152) Scorrano L, Penzo D, Petronilli V, Pagano F, Bernardi P. Arachidonic acid causes cell death through the mitochondrial permeability transition. Implications for tumor necrosis factor-alpha aopototic signaling. *J Biol Chem* 2001 April 13;276(15):12035-40.

(153) Eisenhofer G, Friberg P, Rundqvist B et al. Cardiac sympathetic nerve function in congestive heart failure. *Circulation* 1996 May 1;93(9):1667-76.